



Two-Dimensional Adaptive-Wall Experiments

R. L. Parker, Jr., and W. L. Sickles
ARO, Inc.

February 1981

Final Report for Period October 1979 — September 1980

Approved for public release; distribution unlimited.

**ARNOLD ENGINEERING DEVELOPMENT CENTER
ARNOLD AIR FORCE STATION, TENNESSEE
AIR FORCE SYSTEMS COMMAND
UNITED STATES AIR FORCE**

NOTICES

When U. S. Government drawings, specifications, or other data are used for any purpose other than a definitely related Government procurement operation, the Government thereby incurs no responsibility nor any obligation whatsoever, and the fact that the Government may have formulated, furnished, or in any way supplied the said drawings, specifications, or other data, is not to be regarded by implication or otherwise, or in any manner licensing the holder or any other person or corporation, or conveying any rights or permission to manufacture, use, or sell any patented invention that may in any way be related thereto.

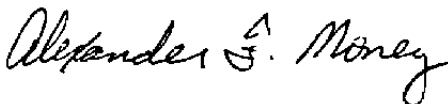
Qualified users may obtain copies of this report from the Defense Technical Information Center.

References to named commercial products in this report are not to be considered in any sense as an indorsement of the product by the United States Air Force or the Government.

This report has been reviewed by the Office of Public Affairs (PA) and is releasable to the National Technical Information Service (NTIS). At NTIS, it will be available to the general public, including foreign nations.

APPROVAL STATEMENT

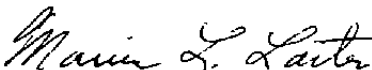
This report has been reviewed and approved.



ALEXANDER F. MONEY
Project Manager
Directorate of Technology

Approved for publication:

FOR THE COMMANDER



MARION L. LASTER
Director of Technology
Deputy for Operations

10

REPORT DOCUMENTATION PAGE		READ INSTRUCTIONS BEFORE COMPLETING FORM
1 REPORT NUMBER AEDC-TR-80-63	2 GOVT ACCESSION NO.	3 RECIPIENT'S CATALOG NUMBER
4 TITLE (and Subtitle) TWO-DIMENSIONAL ADAPTIVE-WALL EXPERIMENTS		5 TYPE OF REPORT & PERIOD COVERED Final Report-October 1979 to September 1980
		6 PERFORMING ORG. REPORT NUMBER
7 AUTHOR(s) R. L. Parker, Jr., and W. L. Sickles, ARO, Inc., a Sverdrup Corporation Company		8 CONTRACT OR GRANT NUMBER(s)
9 PERFORMING ORGANIZATION NAME AND ADDRESS Arnold Engineering Development Center/DOT Air Force Systems Command Arnold Air Force Station, Tennessee 37389		10 PROGRAM ELEMENT PROJECT, TASK AREA & WORK UNIT NUMBERS Program Element 65807F
11 CONTROLLING OFFICE NAME AND ADDRESS Arnold Engineering Development Center/DOS Air Force Systems Command Arnold Air Force Station, Tennessee 37389		12 REPORT DATE February 1981
14 MONITORING AGENCY NAME & ADDRESS (if different from Controlling Office)		13 NUMBER OF PAGES 53
		15 SECURITY CLASS (of this report) UNCLASSIFIED
		15a DECLASSIFICATION DOWNGRADING SCHEDULE N/A
16 DISTRIBUTION STATEMENT (of this Report) Approved for public release; distribution unlimited.		
17 DISTRIBUTION STATEMENT (of the abstract entered in Block 20, if different from Report)		
18 SUPPLEMENTARY NOTES Available in Defense Technical Information Center (DTIC)		
19 KEY WORDS (Continue on reverse side if necessary and identify by block number) porosity plenum walls wings transonic wind tunnels models variable pressure		
20 ABSTRACT (Continue on reverse side if necessary and identify by block number) Experiments conducted in the Arnold Engineering Development Center (AEDC) Propulsion Wind Tunnel Facility Aerodynamic Wind Tunnel (1T) were part of a continuing program to develop adaptive-wall technology for the elimination of wall interference in transonic wind tunnels. The test section arrangement consisted of uniformly variable-porosity porous walls enclosed by a variable pressure plenum. Two subplena were attached to both the top and		

UNCLASSIFIED

UNCLASSIFIED

20. ABSTRACT (Continued)

bottom walls in the region of the test model location. Two subplena locations were investigated. One location was established by test section boundary flow-angle criteria, and the other by test section boundary pressure criteria. The subplena location was shown to significantly affect the results. The test model was a six-percent solid blockage, two-dimensional NACA-0012 wing. The experiments were conducted for both lifting and nonlifting conditions including those conditions for which the supercritical flow regions extended to the test section boundary.

UNCLASSIFIED

PREFACE

The work reported herein was conducted by the Arnold Engineering Development Center (AEDC), Air Force Systems Command (AFSC), for the Directorate of Technology (AEDC/DOT). The results were obtained by ARO, Inc., AEDC Group (a Sverdrup Corporation Company), operating contractor for the AEDC, AFSC, Arnold Air Force Station, Tennessee, under ARO Project Number P32C-36. The Air Force project manager was Mr. Alexander F. Money. The manuscript was submitted for publication on October 21, 1980.

CONTENTS

	<u>Page</u>
1.0 INTRODUCTION	5
2.0 ADAPTIVE-WALL CONCEPT	5
3.0 APPARATUS	
3.1 Aerodynamic Wind Tunnel (IT)	6
3.2 Model	6
3.3 Adaptive-Wall Configuration	7
3.4 Control Surface Measurements	8
3.5 Instrumentation	10
4.0 COMPUTATIONAL METHODS	10
5.0 EXPERIMENTAL PROCEDURE	12
6.0 RESULTS AND DISCUSSION	
6.1 Extended Experiments with Global Wall Control	12
6.2 Subplena Effects	13
6.3 Experimental Results	16
7.0 CONCLUDING REMARKS	17
REFERENCES	18

ILLUSTRATIONS

Figure

1. Basic Iterative Scheme for Adaptive-Wall Concept	21
2. Aerodynamic Wind Tunnel (IT)	22
3. Model Geometry	23
4. Experimental Configuration: Subplena Location by Flow-Angle Strategy	24
5. Experimental Configuration 3: Subplena Location by Pressure Strategy	25
6. Static Pressure Pipe	26
7. Flow-Angle Probe System and Probe Details	27
8. Boundary-Value Problem of Exterior Unconfined Region	29
9. Control Surface Pressure Distribution, $M_\infty = 0.9$ and $\alpha = 0$	30
10. Model Surface Pressure Distribution, $M_\infty = 0.9$ and $\alpha = 0$	31
11. Control Surface Pressure Distribution, $M_\infty = 0.8$ and $\alpha = 0$	32
12. Model Surface Pressure Distribution, $M_\infty = 0.8$ and $\alpha = 0$	33
13. Control Surface Pressure Distribution, $M_\infty = 0.8$ and $\alpha = 0$	34
14. Upper Control Surface Flow-Angle Distribution, $M_\infty = 0.8$ and $\alpha = 0$	35

<u>Figure</u>	<u>Page</u>
15. Model Surface Pressure Distribution, $M_\infty = 0.8$ and $\alpha = 0$	36
16. Control Surface Pressure Distribution, $M_\infty = 0.8$ and $\alpha = 2$	37
17. Control Surface Flow-Angle Distribution, $M_\infty = 0.8$ and $\alpha = 2$	38
18. Model Surface Pressure Distribution, $M_\infty = 0.8$ and $\alpha = 2$	40
19. Control Surface Pressure Distribution, $M_\infty = 0.8$ and $\alpha = 4$	41
20. Control Surface Flow-Angle Distribution, $M_\infty = 0.8$ and $\alpha = 4$	42
21. Model Surface Pressure Distribution, $M_\infty = 0.8$ and $\alpha = 4$	44
22. Control Surface Pressure Distribution, $M_\infty = 0.8$ and $\alpha = 0$	45
23. Upper Control Surface Flow-Angle Distribution, $M_\infty = 0.85$ and $\alpha = 0$	46
24. Model Surface Pressure Distribution, $M_\infty = 0.85$ and $\alpha = 0$	47
25. Control Surface Pressure Distribution, $M_\infty = 0.9$ and $\alpha = 0$	48
26. Upper Control Surface Flow-Angle Distribution, $M_\infty = 0.9$ and $\alpha = 0$	49
27. Model Surface Pressure Distribution, $M_\infty = 0.9$ and $\alpha = 0$	50

TABLES

1. Pertinent Test Data Information	51
--	----

NOMENCLATURE	52
--------------------	----

1.0 INTRODUCTION

Increasingly sophisticated aerodynamic configurations demand higher quality data from transonic test facilities. Inflated energy costs are making smaller facilities more attractive; however, Reynolds number considerations demand larger models. The adaptive-wall concept offers a viable means of satisfying these constraints on transonic wind tunnels. Heretofore, adaptive-wall research has been conducted in two dimensions for the obvious reason of reducing the complexity of the external region computations and the experimental hardware. The development effort at Arnold Engineering Development Center (AEDC) has not been an exception. Some exploratory experiments, however, were conducted for three-dimensional flow in a variable-porosity-wall wind tunnel [AEDC Propulsion Wind Tunnel Facility (PWT) Aerodynamic Wind Tunnel 4T] (see Ref. 1).

The initial AEDC experiments (Ref. 2) applied adaptive-wall techniques to simply adjust the porosity and plenum chamber pressure for a conventional transonic test section arrangement with uniformly variable porosity walls. Successful results were demonstrated through Mach 0.8 and 1-deg model incidence. Subsequent experiments at higher Mach numbers and model incidences revealed the requirement for longitudinally distributed boundary control. Localized boundary control was conveniently obtained by the addition of two subplena on the top and bottom walls in the region of the test section occupied by the model. The experimental development continued with this test section arrangement, including the subplena at two different axial locations. This report summarizes the results of the two-dimensional adaptive-wall development at AEDC.

2.0 ADAPTIVE-WALL CONCEPT

According to the adaptive-wall concept, to ascertain whether unconfined flight conditions are obtained in any wind tunnel, for any model configuration, it must be determined whether the measured flow variables at a convenient surface, S , away from the model and near the walls are consistent with flow in an unconfined region outside the tunnel. To make this determination, the distributions of two flow variables (such as the velocity components parallel and perpendicular to the surface, S) are measured at S ; one is used as the boundary value to specify uniquely the flow field exterior to S at unconfined, undisturbed flow of a uniform stream at infinity. Since the two measured distributions constitute redundant boundary data in the presence of the exterior region, far-field, boundary condition, equality at S of the measured flow variables interior to S and the computed flow variables exterior to S constitutes a definition of interference-free flow in the wind tunnel. Therefore, by comparing the exterior region calculated values to the measured values of the same quantities, it can be determined whether unconfined flow conditions exist in the tunnel.

Unconfined flow conditions can be achieved if provisions are made for adjusting the wall boundary as necessary. A basic iterative scheme for applying the adaptive-wall technique to achieve unconfined flow is presented in Fig. 1. The axial and normal components, u and v , respectively, of the disturbance velocity are assumed to be the flow variables of interest at S . First, a flow field is established in the tunnel, and the velocity components u_T and v_T are measured at the given control surface, S . The exterior unconfined region is then evaluated by specifying $v_E = v_T$ as the boundary value at S . If the distribution at S of u_E determined from the exterior region calculation does not agree with u_T , then the flow is still constrained at the walls and the wall boundary must be readjusted. The iteration continues until u_E and u_T agree. Then the flow about the model in the tunnel is unconfined. The relaxation factor, k , is introduced to accelerate convergence of the iterative procedure as discussed in Ref. 3.

Alternatively, $u_E = u_T$ could be specified at S in the exterior region and v_E compared with v_T to determine whether unconfined flow exists in the tunnel. More generally, any two conveniently measured flow variables can be used in the adaptive-wall process. The approach is valid for both two- and three-dimensional flow fields.

In addition to the standard equipment for wind tunnel testing, application of the adaptive-wall concept requires the following: (1) adaptive wall, (2) measurement devices for two flow variables at the reference surface, S , and (3) a computational capability for evaluating the requisite functional relationships for the two flow variables in the unconfined external regions.

3.0 APPARATUS

3.1 AERODYNAMIC WIND TUNNEL (1T)

The experiments were conducted in the Aerodynamic Wind Tunnel (1T), which is a continuous-flow, nonreturn wind tunnel equipped with a two-dimensional, flexible nozzle and an auxiliary plenum evacuation system. The test section is of square cross section nominally 12 in. square and 37.5 in. long. The tunnel is operated at a total pressure of approximately 2,850 psfa. The stagnation temperature can be varied from 80 to 120°F above ambient temperature to prevent visible condensation from occurring in the test section. The tunnel arrangement is shown in Fig. 2.

3.2 MODEL

For these experiments with the adaptive-wall concept, a two-dimensional model was selected to comply with existing computational techniques and to minimize complexity of

wall hardware and reference plane measuring devices. A 6-in.-chord NACA 0012 airfoil was chosen for the following reasons:

1. The NACA 0012 profile has been shown to be relatively insensitive to Reynolds number effects above 2×10^6 chord Reynolds number (Ref. 4).
2. The profile shape and size are equivalent to the model used in the Calspan experiments (Ref. 5), and, hence, surface pressure data from Ref. 6 could be used for comparison.
3. The profile shape and size (6-percent blockage) should produce significant wall interference effects at transonic speeds.

The geometric details and locations of static pressure orifices on the model are illustrated in Fig. 3.

3.3 ADAPTIVE-WALL CONFIGURATION

For practical applications, three distinct methods for producing adaptive-wall control exist: (1) localized plenum pressure control, (2) localized wall contour control (streamlined walls), and (3) local wall crossflow characteristics control. In addition, some combination of these methods could be used. Method 1 has been investigated in Refs. 5 and 7, and method 2 has been investigated in Refs. 8, 9, and 10.

The philosophy adopted for the present development at AEDC is to employ a method of wall control that requires minimum modification to existing wind tunnel test sections. Reference 2 reported the first phase of the development in which adaptive techniques were employed simply to adjust the plenum suction and the porosity of a uniformly variable porosity wall. A second wall configuration was also investigated that incorporated the capability of locally adjusting the porosity. This was accomplished by sandwiching bored spheres between porous plates. Individual rotation of rows of spheres made it possible to change the hole angle and, hence, the crossflow characteristic. As reported in Ref. 2, this wall configuration offered little advantage over the uniformly variable porosity wall. The variable-porosity wall, in conjunction with the single, main plenum chamber surrounding the test section, will be referred to hereafter as Configuration 1.

It was also reported in Ref. 2 that a major criterion to match on the pressure distribution at the control surface was the location and magnitude of the minimum pressure region or peak region in order to minimize interference at the model location. Configuration 1 was quite effective for adjusting the control surface peak region and, when the peak region was

adjusted correctly, the upstream and downstream regions of the pressure distribution were reasonably approximated for Mach numbers below 0.8. As test conditions with larger flow perturbations were approached, however, it became apparent that better control resolution was required. This will be discussed in detail in Section 6.1.

For a typical distribution of the flow angle near the wall, there is a region of large outflow from the test section near the model leading-edge location and a large region of inflow into the test section near the model trailing-edge location. Analysis of the first phase experimental results indicated that the wall control could be enhanced by the addition of two subplena — one to control the outflow region and one to control the inflow region. The resulting configuration is shown in Fig. 4. The two subplena were divided at the tunnel station corresponding to the model quarter-chord, approximately where the flow angle is zero. The arrangement shown in Fig. 4 is referred to as Configuration 2. There was a manifold for the upper and lower pairs of subplena in which the pressure could be adjusted. Each subplenum could be controlled independently. The top and bottom pairs of subplena could also be controlled as units since they were connected via a manifold to evacuation lines. Therefore, the pressure in each pair of plena could be adjusted either collectively (for the pair) or individually (for each plenum) as required. The rear plenum on both top and bottom could also be vented to atmosphere, thereby providing blowing into the test section.

Analysis of the results employing Configuration 2 indicated that additional control was required in the region of the peak control surface pressure, which corresponds to the zero flow-angle location. This observation led to Configuration 3 (Fig. 5). Configuration 3 is similar to Configuration 2 with the subplena repositioned so that the upstream plena are centered in the region of additional required pressure control.

3.4 CONTROL SURFACE MEASUREMENTS

Implementation of the adaptive-wall technique requires the measurement of two flow variables at a reference surface (control surface), S , near the tunnel boundary. For a two-dimensional model experiment, the surface, S , is conveniently defined by two surfaces ($y = \pm h$) parallel to the tunnel axis near the upper and lower walls. In the present study, the flow variables of interest are the perturbation velocities parallel and normal to the control surface, u and v , respectively. In practice, the static pressure and flow angle along the control surface were measured, and the linearized relations given in Section 4 were used to convert them to the perturbation velocities.

The distribution of static pressure at the control surface was measured by a 0.5-in.-diam static pipe parallel to the tunnel centerline. Details of the static pipe installation and locations of the orifices are shown in Fig. 6. The static pipe had 30 orifices oriented toward the plane of the wing. The pressure coefficient from the pressure measurement of the pipe is accurate to within ± 0.01 .

The distribution of the flow angle along the control surfaces was obtained by traversing flow angularity probes longitudinally along the planes of the upper and lower control surfaces. The flow-angle probe system and probe details are shown in Fig. 7. The traversing system can position the probes, one each along the upper and the lower control surface, continuously from tunnel station 5 to station 31. The drive mechanism was mounted on the plenum side of the test section side wall. The probes were mounted to wedge-shaped struts that protruded through slots in the side wall. The side wall slots were isolated from the plenum chamber so that the pressure behind the slot would be equal to the test section static pressure.

Four flow angularity probes were fabricated for these experiments. Two probes were hemispherical head probes and two were 20-deg-included-angle conical head probes. Each type had a cylindrical body. The hemispherical head probes had four pressure orifices spaced and evenly located radially 45 deg on the surface from the probe tip. The conical head probes had four pressure orifices equally spaced and located radially 60 percent of the cone length aft of the probe tip.

The flow angularity probes were individually calibrated to determine their sensitivity ($\Delta\theta/\Delta P$) and were accurate to within ± 0.1 deg. The probes were then installed on the traversing system in the tunnel test section. The perforated walls were closed to yield zero porosity. With the tunnel test section empty, the probes were traversed from tunnel station 5 to station 31 at Mach numbers from 0.5 to 0.95. The tunnel flow was assumed to be parallel to the walls. The installation offset angle for each probe and the variation of the offset with axial motion were determined, and appropriate corrections were applied to the measurements during the adaptive-wall experiments. The flow angle at the control surface could be determined to within ± 0.2 deg.

When the experiments began, hemispherical head probes were installed. Shortly after the experiments began, the lower hemispherical head probe developed an internal pressure leak and was replaced with a conical head probe. All of the experiments reported herein were conducted with the latter probe arrangement, consisting of a hemispherical head probe on the upper surface and a conical head probe on the lower surface.

3.5 INSTRUMENTATION

The standard Tunnel IT instrumentation was used to measure plenum chamber pressure (P_c), tunnel total pressure (P_T), and tunnel total temperature (T_O). The pressure at the flow angularity probe orifices was measured by strain-gage-type differential pressure transducers. Static pressure on the model and on the control surface was measured by 15-psid transducers using Scanivalves®. The data were recorded by a computer system that reduced the data to engineering units, computed pertinent parameters, and tabulated the results.

4.0 COMPUTATIONAL METHODS

The principal theoretical aspect of the adaptive-wall method is the evaluation of the functional relationships that satisfy the conditions for unconfined flow in the region exterior to S (as shown in Fig. 8). This requires the solution of the flow field exterior to the interface with the distribution of one of the measured flow variables prescribed as the boundary condition. Since the region exterior to S contains no immersed bodies (and, hence, no boundary layer), and since S is presumed sufficiently removed from the experimental model so that disturbances from the model have weakened, the application of inviscid, small-disturbance theory to the exterior region appears justified.

Consistent with the small-disturbance approximation, it was found convenient to work in terms of the nondimensional disturbance velocity components, u and v , streamwise and normal, respectively, to the reference surface, S . Since static pressure and flow-angle distributions were measured at S , the linear approximations $u = -C_p/2$ and $v = \theta$ were utilized. Preliminary studies of the adaptive-wall concept showed that it would be advantageous to use v as the boundary condition in the external region and to use u as the parameter to adjust the tunnel boundaries. The primary reason for assigning these functions to u and v is that the flow in the tunnel appears to be more sensitive to changes in pressure (or u) than to changes in flow direction (or v). Details of the relative sensitivity of u and v are given in Ref. 11.

In the present study, two techniques were used to evaluate the requisite functional relationships at the interface, S . The first technique is based on the one-step convergence formulas derived in Ref. 12. The resulting expressions are

$$u_{\infty}(x, \pm h) = \frac{1}{2} u_T(x, \pm h) - \frac{\beta h}{\pi} \int_{-\infty}^{\infty} \frac{u_T(\xi, \mp h)}{k(\xi - x)} d\xi \\ \mp \frac{1}{2\pi\beta} \oint_{-\infty}^{\infty} \frac{v_T(\xi, \pm h)}{\xi - x} d\xi \pm \frac{1}{2\pi\beta} \int_{-\infty}^{\infty} \frac{v_T(\xi, \mp h)}{k(\xi - x)} (\xi - x) d\xi \quad (1)$$

and

$$v_{\infty}(x, \pm h) = \frac{1}{2} v_T(x, \pm h) - \frac{\beta h}{\pi} \int_{-\infty}^{\infty} \frac{v_T(\xi, \mp h)}{k(\xi - x)} d\xi \\ \pm \frac{\beta}{2\pi} \int_{-\infty}^{\infty} \frac{u_T(\xi, \pm h)}{\xi - x} d\xi \mp \frac{\beta}{2\pi} \int_{-\infty}^{\infty} \frac{u_T(\xi, \mp h)}{k(\xi - x)} (\xi - x) d\xi \quad (2)$$

where $k(\xi - x) = (2\beta h)^2 + (\xi - x)^2$, $y = \pm h$ are the reference surfaces, S , for the two-dimensional application, and $\beta = (1 - M_{\infty}^2)^{1/2}$. The integrals in Eqs. (1) and (2) are evaluated by simple quadrature using the curve-fitted values of the measured values of u_T and v_T . The one-step equations are based on linearized Prandtl-Glauert theory and are applicable, provided that the flow is subcritical at the interface. When these expressions are used, the number of adaptive-wall iterations required to determine unconfined conditions is significantly reduced, and, under certain stipulations, unconfined flow conditions are determined directly once u_T and v_T have been measured.

If supercritical flow exists near the measuring surface, S , it is necessary to account for discontinuities in the flow field with a nonlinear theory. In the present study, a conservative mixed-operator, finite-difference scheme was used to solve the transonic small-disturbance equation

$$\left[\beta^2 \phi_x - \frac{\gamma + 1}{2} M_{\infty}^2 \phi_x^2 \right]_x + [\phi_y]_y = 0 \quad (3)$$

where ϕ is the velocity potential.

Equation (3) was approximated by difference equations in the exterior region with a 63-by 56-non-uniform grid mesh. The difference equations are developed using central difference operators in the subsonic region, upwind difference operators in the supersonic region, and a shock operator to give the correct jump condition. The measured distribution of flow angle, v_T , was smoothed and curve-fitted to provide the boundary condition at $y = \pm h$. Uniform flow, $C_p = 0$, was used as the boundary condition on the other boundaries of the computational domain. This boundary value problem is solved using the iterative technique of successive line over-relaxation. The iteration is continued until the maximum residual of the velocity potential is less than 1×10^{-4} . The value of u_E is then determined as x at the control surface.

As discussed in Ref. 3, the average of the measured velocity, u_T , and the calculated velocity, u_E , provides a good approximation to conditions for unconfined flow. In addition, as convergence to unconfined flow is approached, the result of the one-step formula, u ,

should be identical to the exterior solution, u_E . During the test program, u , derived from the one-step formula [Eq. (1)], was used to adjust the tunnel boundary as long as the flow at the control surface remained subcritical. At higher Mach numbers, the average of the measured value, u_T , and external finite difference solution, u_E , was used as the criterion for adjusting the tunnel boundaries.

5.0 EXPERIMENTAL PROCEDURE

The wind tunnel top and bottom test section walls were aligned parallel and level. The two-dimensional NACA 0012 wing model, which spanned the tunnel test section, was adjusted to within ± 0.1 deg of the desired angle of attack, defined as the angle relative to the tunnel horizontal axis. All data were obtained with natural boundary-layer transition on the wing model. The test unit Reynolds number varied from nominally 4×10^6 to 4.8×10^6 per foot, depending on Mach number.

The test Mach number was defined and input to the online data reduction program. The pressure on the model surface and on the adaptive-wall control surface was converted to coefficient form based on the defined Mach number. A flow was established in the test section at the pressure ratio across the test section specified by the tunnel-empty calibration for the defined Mach number. The main plenum and subplena pressures were also adjusted to the value specified by the tunnel-empty calibration for the initial case, or 0th iteration. For subsequent iterations the main plenum pressure was allowed to remain at the value specified by the calibration. The subplena pressures, however, were adjusted to obtain the best match of the control surface pressure distribution with that computed for the exterior, unconfined region.

6.0 RESULTS AND DISCUSSION

6.1 EXTENDED EXPERIMENTS WITH GLOBAL WALL CONTROL

The results of the adaptive-wall experiments with variable-porosity walls with a single plenum chamber (i.e., Configuration 1) were reported in Ref. 2. This configuration is described as having global control since the plenum pressure behind the wall and the porosity of the wall is uniform everywhere. The experiments reported in Ref. 2 included test conditions through Mach number 0.8 and model incidence of 1 deg with generally successful results.

Subsequent experiments were conducted in which the test conditions were extended to higher Mach numbers and model incidences. As the test conditions were expanded, the

demand for local boundary control, distributed wall control, became increasingly evident. It was observed in the early AEDC adaptive-wall experiments and reported in Refs. 1 and 2 that the control surface pressure distribution could be considered to have three critical regions where the measured and computed pressures were required to be in agreement. The most important region is that near the model, or peak region; second is the upstream region, where the correct free-stream Mach number is required; and third is the downstream region, where the flow should return to free-stream conditions. All of these requirements could be established with global control at the conditions approached in the early experiments (Ref. 2). As more demanding test conditions were approached, it was found that, when the pressure in the peak region was adjusted as required, the upstream and downstream conditions were not at the required values. An example is given in Fig. 9 in which the pressure distribution on the control surface is shown for Mach 0.9 and a model incidence of 0 deg. At these conditions the control surface pressure could not be simultaneously matched in all three regions to that computed for unconfined flow. When the plenum suction was adjusted to lower the pressure in the peak region, the flow upstream and downstream of the model was accelerated to above the value for $M_\infty = 0.9$. No combination of plenum pressure and wall porosity was found to improve these results. The corresponding model pressure distribution is shown in Fig. 10. The reference data which were assumed to be interference free were obtained on a similar model in the Calspan 8-ft Transonic Wind Tunnel (Ref. 6). As shown in the figure, the pressure distribution for Configuration 1 is consistent with the control surface information in Fig. 9 in that the pressure from the 25- through 70-percent chord locations shows significant interference and the shock location is too far downstream.

6.2 SUBPLENA EFFECTS

A subplena arrangement was added to the top and bottom walls in the model vicinity to acquire better resolution of the boundary control or axially distributed control. The first subplena arrangement (Configuration 2) consisted of two subplena positioned according to the flow-angle distribution at the test section boundary (see Section 3.3). With this arrangement, the boundary characteristics in the peak region could be independently controlled (i.e., independent of the characteristics upstream and downstream of the model location).

A comparison of the results for Configurations 1 and 2 is shown in Figs. 11 and 12. The pressure distribution along the control surface for $M_\infty = 0.8$ and $\alpha = 0$ deg is shown in Fig. 11 for the standard tunnel configuration consisting of a uniform porosity distribution of 4 percent and the plenum pressure adjusted according to the empty tunnel calibration. Configuration 1 corresponds to a uniform wall porosity of 4 percent and a uniform plenum pressure adjusted according to the adaptive-wall control surface criteria. Configuration 2 consists of a uniform wall porosity of 4 percent with the main plenum adjusted according to

the empty tunnel calibration value and the pressure in the subplena adjusted to obtain the best agreement of the computed and measured control surface flow variables. A uniform wall porosity of 4 percent was selected for the comparison because this porosity yielded the best results for Configuration 1 (Ref. 2).

The addition of the subplena offered several advantages over Configuration 1. The "trailing-off" of the pressure distribution at the downstream end of the test section for Configuration 1 was caused by a reduction in the pressure ratio that was necessary for properly positioning the terminal shock on the model (Ref. 2). This was required at Mach numbers of 0.8 and above. All the experiments with Configurations 2 and 3, with the subplena, were conducted at the standard test section pressure ratio as determined by the empty tunnel calibration. The control surface pressure distribution for Configuration 2 (Fig. 11) was obtained with adjustments to the subplena only. The large blockage effects of the model could, therefore, be removed by local boundary adjustments about the model. When the adjustments were made with the subplena pressure control, the approaching free-stream Mach number was maintained at the correct value with the main plenum at the empty tunnel calibrated value. The results with Configuration 2, however, showed no improvement over those for Configuration 1 in matching the computed unconfined pressure distribution in the regions just upstream and downstream of the peak region, about X/C locations -0.3 and 1.0, respectively. As discussed in Refs. 1 and 2, it is not critical to match the pressure distribution for unconfined flow in these regions to obtain essentially unconfined flow results at the model location.

The pressure distribution on the model surface corresponding to the control surface information in Fig. 11 is shown in Fig. 12. Included in the figure are reference data from Ref. 6 and data for NACA-0012 wing sections tested in the NAE 5 x 5 trisonic and Modane S3 wind tunnels (Ref. 14). Additional information concerning these data is contained in Table 1.

Additional experimental results with Configuration 2 were obtained at higher Mach numbers and model incidences. As discussed in Section 3.3, the criterion for positioning and determining the axial length of the subplena was based on test section boundary flow-angle variation. The forward subplenum was positioned to control the region of large outflow from the test section near the model leading edge. The aft subplenum was positioned to control the region of large inflow to the test section near the model trailing edge. Analysis of the results obtained with Configuration 2 indicated that sufficient control was not available in the region of the minimum pressure, or the peak region. This region also corresponds to the region where the flow angle changes signs with the minimum pressure point corresponding to the 0-deg flow-angle location. This also corresponds to the demarcation

between the forward and aft subplena. To enhance the control in the peak region, then, the subplena were translated downstream approximately 2 in. so that the forward plenum would encompass all the peak region (Fig. 5) (Configuration 3).

Comparisons of the results for the two subplena configurations are shown in Figs. 13, 14, and 15. The control surface pressure distribution for Mach 0.8 and 0-deg model incidence is shown in Fig. 13. The results for Configuration 3 show better agreement between the measured control surface pressure and the computed unconfined pressure.

Configuration 3 also provided a better flow-angle distribution, as shown in Fig. 14. The measured flow angles are compared to those computed for unconfined flow using the one-step formulas. For the standard tunnel configuration, outflow from the test section (positive flow angle for the upper control surface) is shown increasing from $X/C = -2$ to -1 , where it became constant at about 1 deg downstream to $X/C = 0$. There are no sharp increase and decrease in flow angle as there are for the computed distribution from $X/C = -1$ to 0. The remainder of the flow-angle distribution downstream of $X/C = 0$ for the standard configuration is in reasonable agreement with the computed flow angle. The effect of Configuration 2 was to increase the flow angle, or outflow, in the region of the forward subplena from $X/C = -1$ to 0. When the subplena were adjusted to match the pressure in the peak region, the flow angle downstream of $X/C = 1$ was too positive, as compared with the computed value. The pressure coefficient (Fig. 13) in the same region is too negative. Any adjustments to the downstream subplena to increase the control surface pressure in this region propagated upstream to the peak region also. The flow-angle distribution for Configuration 3 shows the best agreement with the computed flow angle, both in magnitude and in longitudinal variation. The small forward displacement of the position of the maximum positive flow angle is typical for all Mach numbers and model incidences for which one-step computations can be made.

The model pressure distribution is shown in Fig. 15. Configurations 2 and 3 yield the same results — essentially unconfined flow — at the model, demonstrating again that small discrepancies in the noncritical regions at the control surface can be permitted, since wall interference is maximum at the wall and diminishes with distance from the wall, hence, not affecting the flow at the model location. All of the boundary adjustments were accomplished with suction through both the front and rear subplena. In fact, for all test conditions approached in this study, suction was always required in the forward subplenum and either suction or no mass flow was required in the aft subplenum. When blowing through the rear subplenum was attempted, the effects propagated upstream through the peak region.

The results demonstrated in Figs. 13, 14, and 15 are typical for Configurations 2 and 3. Configuration 3 provided better resolution in both flow angle and pressure at the control surface. Thus, it is concluded that model location relative to the subplena locations can be significant for adaptive-wall test sections with segmented plena boundary control. Configuration 3 also provided increased control magnitude, allowing iterative adaptive-wall adjustments to be made to converge at test conditions of higher Mach numbers and model incidences. The remainder of this discussion will be limited to results obtained with Configuration 3.

6.3 EXPERIMENTAL RESULTS

The test conditions of $M_\infty = 0.8$ and $\alpha = 2$ deg incidence offer a lifting case in which the flow is supercritical on the model upper surface but subcritical at both the upper and lower control surfaces (Fig. 16). The figure includes the computed pressure distribution corresponding to unconfined flow as well as data for Configuration 3 and the standard tunnel configuration consisting of uniform 5-percent-porosity porous walls with uniform pressure in both the main plenum and subplena. The adjustments were made in one iteration by first adjusting the top wall by the upper control surface pressure criteria and the bottom wall by the lower control surface pressure criteria. There was negligible coupling between the top and bottom walls. The corresponding change in the flow-angle distribution along the control surface is shown in Fig. 17. The adjustments to the pressure distribution are directly reflected in the flow-angle distribution. The decrease in pressure in the upper surface peak region about $X/C = 0.4$ is accompanied by increased outflow about $X/C = 0$. The general overall decrease in pressure along the lower control surface corresponds to an overall increase in outflow. The model surface pressure distribution is shown in Fig. 18. The reference data from Calspan (Ref. 6) are shown in Fig. 18 along with data recently obtained at NASA-LRC. A summary of pertinent information concerning the test data is contained in Table 1. The model surface pressure distribution for the configuration adjusted by adaptive techniques is in good agreement with the Calspan data and in excellent agreement with the NASA-LRC data. Reynolds number effects are apparent when comparing the pressure distribution with the Calspan data, which display trailing-edge separation.

The control surface pressure distribution for $M_\infty = 0.8$ and $\alpha = 4$ deg is shown in Fig. 19. At these conditions, the flow at the upper control surface is nearly supercritical. Again, the standard tunnel configuration is a uniform 5-percent-porosity porous wall with a uniform pressure in all the plena equal to the empty tunnel calibrated value. The unconfined flow pressure distribution was computed with use of the one-step formulas. By adjusting the subplena pressure, the control surface pressure distribution for Configuration 3 was obtained in one iteration. The main plenum pressure was maintained at the empty tunnel

calibrated value. Figure 20 shows the corresponding flow-angle distribution at the control surface. The adjustments to the pressure distribution (Fig. 19) corresponded to small changes in the flow-angle distribution (Fig. 20). The model surface pressure distribution is shown in Fig. 21. Configuration 3 gives excellent agreement with the reference data from NASA-LRC. The Reynolds number effects become very apparent at these conditions with the data from Calspan obtained at the lower Reynolds number showing significant separation aft of the shock location. The trailing-edge separation is probably responsible for the forward displacement of the shock position.

The flow at the control surface is critical about the model for $M_\infty = 0.85$ and $\alpha = 0$ deg. The control surface pressure distribution for these conditions is shown in Fig. 22. Again, the adjusted pressure distribution for Configuration 3 was obtained in one iteration using the one-step formulas to compute the pressure distribution corresponding to unconfined flow. The one-step formulas proved to be valid for this case even though the flow was critical over a small portion of the control surface. The standard tunnel configuration is a uniform 5-percent-porosity with a uniform plenum pressure set at the empty tunnel calibrated value. The corresponding flow-angle distribution is presented in Fig. 23, and the model surface pressure distribution is shown in Fig. 24. As Fig. 24 shows, the Configuration 3 model data are in very good agreement with the reference data from NASA-LRC.

Experiments were also conducted at $M_\infty = 0.9$ and $\alpha = 0$ deg. The control surface pressure distribution for these conditions is shown in Fig. 25. The flow is supercritical at the control surface over the length of the model. The data for Configuration 3 are the first iterative step. This was the limit of control available with maximum flow removal through the subplena. The computed pressure distribution for unconfined flow is the finite difference solution corresponding to the first iterative step. Considering a relaxation factor of 0.5, the adjusted wall distribution in the peak region is close to that required for unconfined flow. The corresponding control surface flow-angle distribution is shown in Fig. 26, and the model surface pressure distribution is presented in Fig. 27. The model surface pressure data are consistent with the control surface information. This indicates that the adjusted configuration has nearly achieved the unconfined flow results. The data are compared with the Calspan data. No data were available at this Mach number from NASA-LRC.

7.0 CONCLUDING REMARKS

The first phase of the adaptive-wall experiments at AEDC, reported in Ref. 2, indicated that significant results could be obtained using adaptive techniques to simply adjust uniformly variable porosity walls in conjunction with the plenum pressure to remove wall

interference on a 6-percent solid blockage, 2-D NACA-0012 wing model. Subsequent experiments at higher Mach numbers and model incidences revealed the requirement for localized boundary control, particularly about the model location. Adjusting the uniform boundary control by control surface criteria near the model (the peak region) resulted in incorrect control surface characteristics upstream and downstream of the model. A facilitative means of obtaining the additional localized boundary control was the addition of two independently controlled subplena on both the top and bottom walls. The subplena were originally positioned according to the flow-angle distribution along the test section boundary. The forward subplenum was positioned to influence the region of large outflow from the test section near the model leading edge, and the aft subplenum was positioned to influence the region of large inflow into the test section near the model trailing edge. The aft subplena could also supply blowing into the test section from an atmospheric air supply although it should be noted that blowing into the test section was never required. The required control surface conditions were sufficiently matched with either mass flow removal or no mass flow through the subplena evacuation lines.

Adjustments to the flow could be made adaptively with the subplena. Without exception, the pressure required in the main plenum influencing the flow upstream and downstream of the model corresponded to the empty tunnel calibrated value. Analysis of the results from these experiments indicated that the subplena effectiveness could be enhanced by locating the subplena according to the pressure distribution along the test section boundary. Additional control was required in the region near the minimum control surface pressure location or peak region. Therefore, the subplena were repositioned in accordance with these criteria. The results of the modified configuration were positive and indicated that, for adaptive-wall test sections with subplena boundary control, the size and location of the subplena relative to the model are significant.

REFERENCES

1. Parker, R. L., Jr., and Sickles, W. L. "Application of Adaptive Wall Techniques in a Three-Dimensional Wind Tunnel with Variable Wall Porosity." AIAA Paper No. 80-0157. Presented at AIAA 18th Aerospace Sciences Meeting, Pasadena, California, January 14 — 16, 1980.
2. Kraft, E. M. and Parker, R. L., Jr. "Experiments for the Reduction of Wind Tunnel Wall Interference by Adaptive-Wall Technology." AEDC-TR-79-51 (AD-A076555), October 1979.
3. Lo, C. F. and Kraft, E. M. "Convergence of the Adaptive-Wall Wind Tunnel." *AIAA Journal*, Vol. 16, No. 1, January 1978, pp 67-72.

4. Ponteziere, J. and Bernard-Guelle, R. "E'tude Experimentale des Corrections de Parois a Rich." *L'Aeronautique et l'Astronautique*, No. 32, 1971, pp. 41-52.
5. Erickson, J. D., Jr., Witliff, C. E., and Daughtry, D. C. "Further Investigation of Adaptive-Wall Wind Tunnels." AEDC-TR-80-34, November 1980.
6. Vidal, R. J., Catlin, P. J., and Chudyk, D. W. "Two-Dimensional Subsonic Experiments with an NACA 0012 Airfoil." Calspan Report No. RK-5070-A-3, December 1973.
7. Bodapate, S., Schairer, E. and Davis, S. "Adaptive Wall Wind Tunnel Development for Transonic Testing." AIAA Paper No. 80-0441. Presented at AIAA 11th Aerodynamic Testing Conference, Colorado Springs, Colorado, March 18 — 20, 1980.
8. Goodyer, M. J. and Wolf, S. W. D., "The Development of a Self-Streamlining Flexible Walled Transonic Test Section." AIAA Paper No. 80-0440. Presented at AIAA 11th Aerodynamic Testing Conference, Colorado Springs, Colorado, March 18 — 20, 1980.
9. Chevallier, Jean-Pierre. "Soufflerie Transonique a Parois Auto-Adaptables." AGARD Conference Proceedings No. 174 — Wind Tunnel Design and Testing Techniques, Paris (France), March 1976.
10. Ganzer, Vwe. "Wind Kanale mit adaptiven Wanden zur Beseitigung von W and inter ferenzer." Zeitschrift fur Flugwissenschaften and Weltraum for schung, 3 (1979), Heft 2.
11. Vidal, R. J. and Erickson, J. D., Jr., Calspan Corporation. "Research on Adaptive Wall Wind Tunnels." AEDC-TR-78-36 (AD-A062110), November 1978; Calspan Report No. RK-5934-A-1.
12. Lo, C. F. and Sickles, W. L. "Analytic and Numerical Investigation of the Convergence for the Adaptive Wall Concept." AEDC-TR-79-55 (AD-A078203), November 1979.
13. "Experimental Data Base for Computer Program Assessment," Report of the Fluid Dynamics Panel Working Group, Advisory Group for Aerospace Research and Development. AGARD-AR-138, May 1979.
14. Jacocks, J. L., Sinclair, D. W., and Parker, R. L., Jr. "Evaluation of the Acoustic and Aerodynamic Characteristics of Several Slot-Baffle Configurations for Transonic Wind Tunnel Walls." AEDC-TR-79-59.

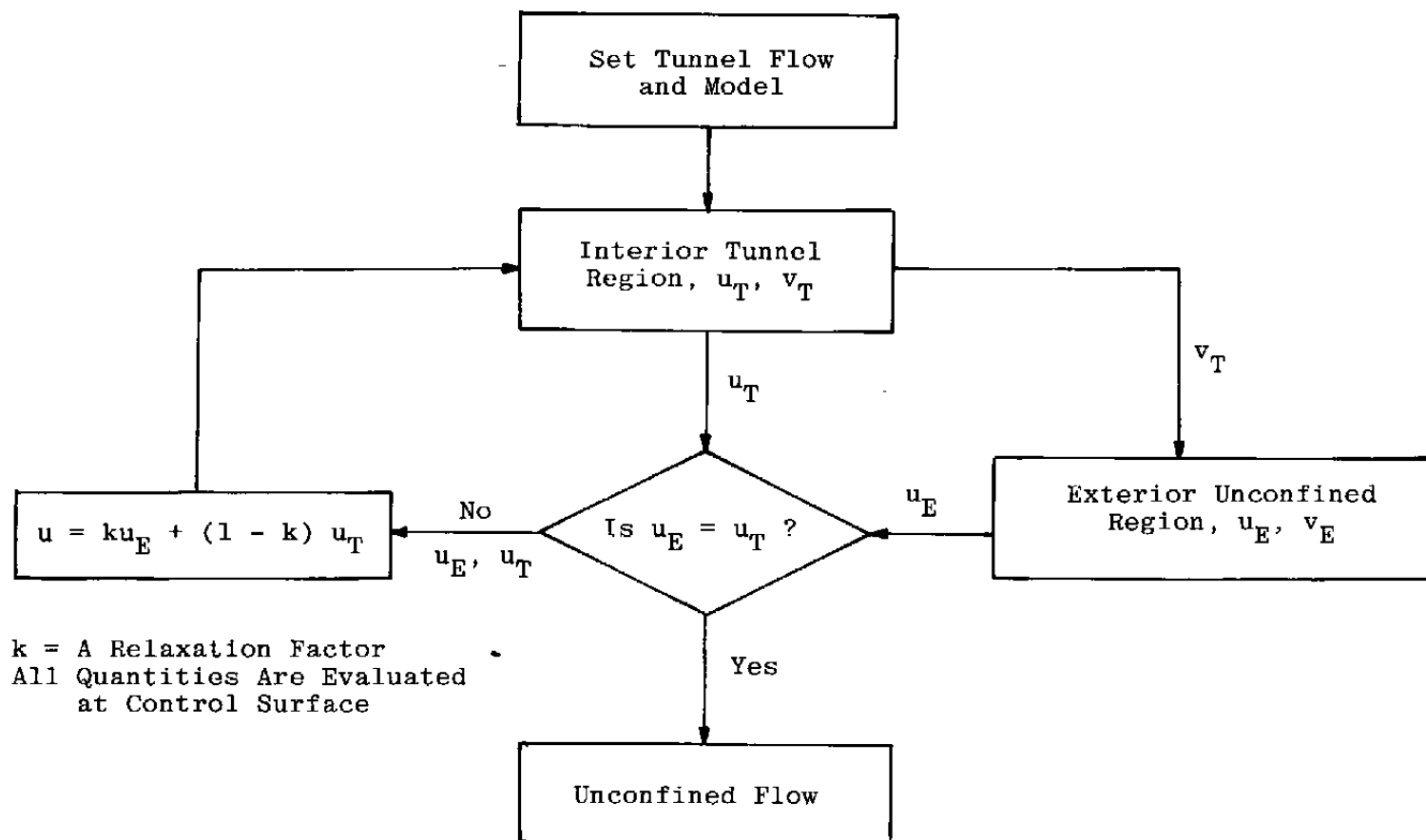


Figure 1. Basic interactive scheme for adaptive-wall concept.

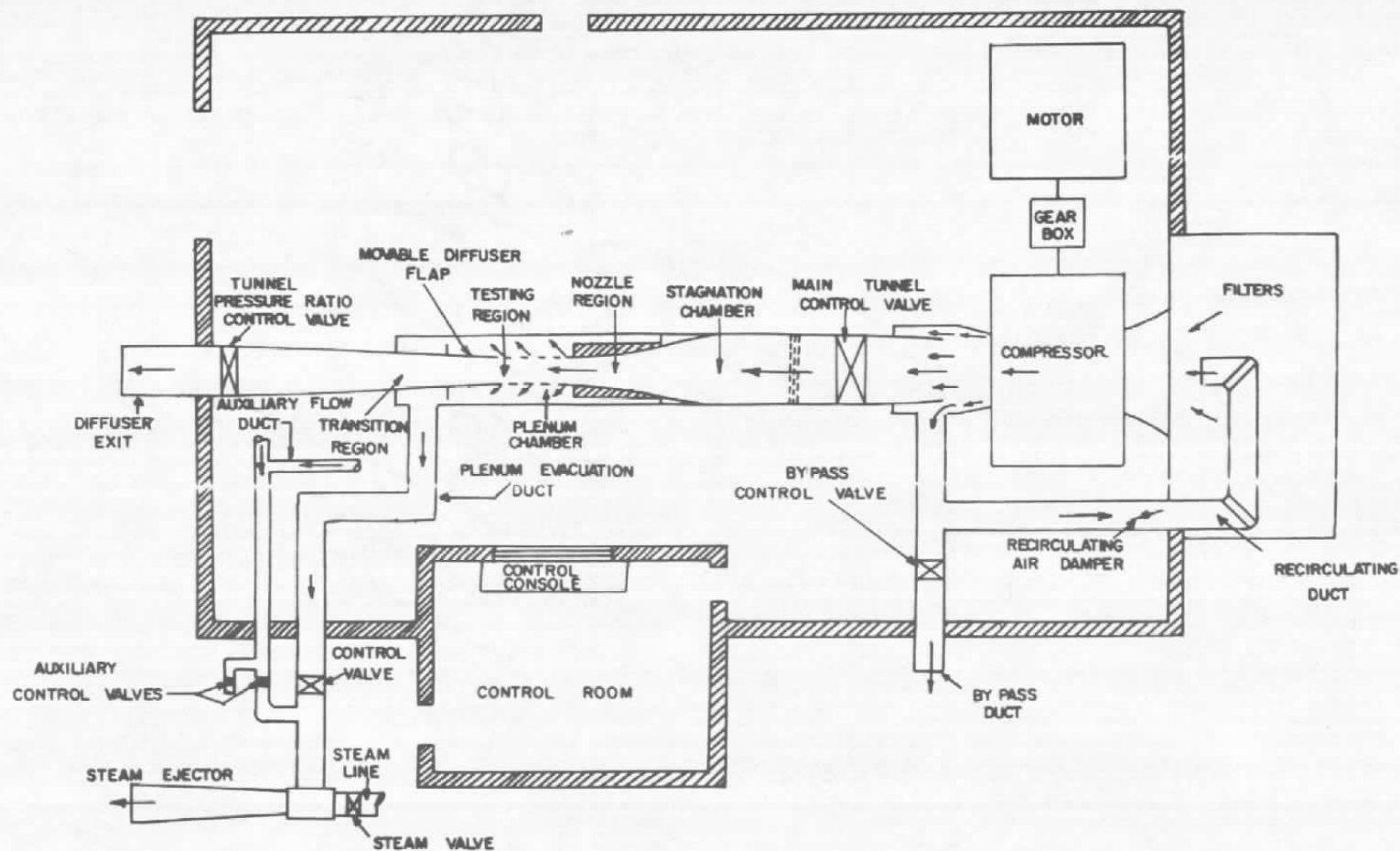
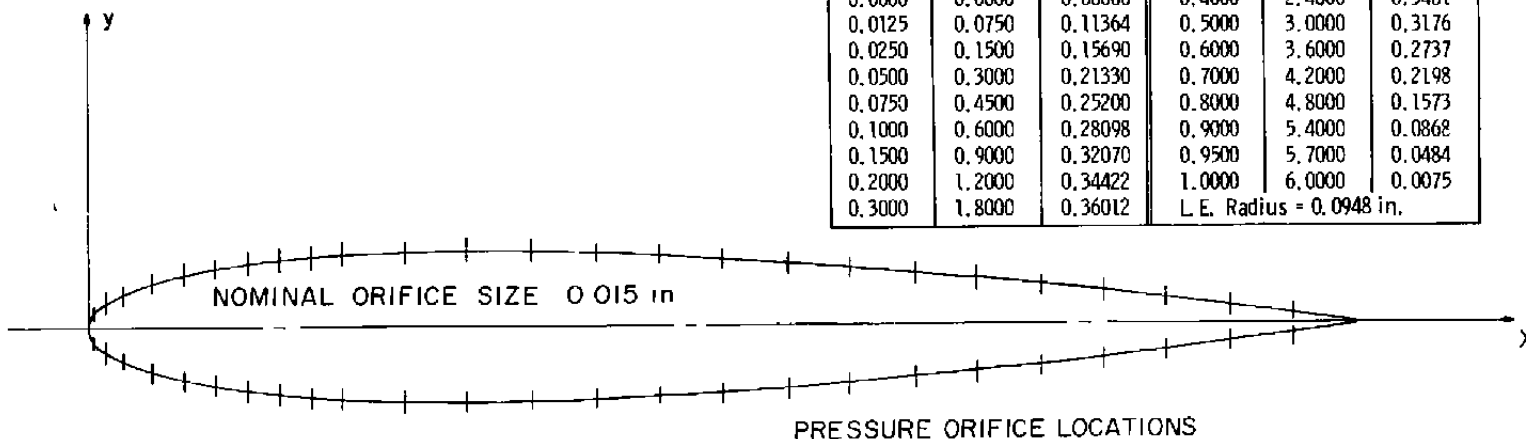


Figure 2. Aerodynamic Wind Tunnel (1T).

PROFILE GEOMETRY. $\pm y = 0.72(1.4845\sqrt{X} - 0.6300X - 1.7580X^2 + 1.4215X^3 - 0.5075X^4)$, in.

X/c	X, in	$\pm y$, in	X/c	X, in	$\pm y$, in
0.0000	0.0000	0.00000	0.4000	2.4000	0.3481
0.0125	0.0750	0.11364	0.5000	3.0000	0.3176
0.0250	0.1500	0.15690	0.6000	3.6000	0.2737
0.0500	0.3000	0.21330	0.7000	4.2000	0.2198
0.0750	0.4500	0.25200	0.8000	4.8000	0.1573
0.1000	0.6000	0.28098	0.9000	5.4000	0.0868
0.1500	0.9000	0.32070	0.9500	5.7000	0.0484
0.2000	1.2000	0.34422	1.0000	6.0000	0.0075
0.3000	1.8000	0.36012	L. E. Radius = 0.0948 in.		



X/c	X, in	X/c	X, in
0.0000	0.0000	0.3500	2.100
0.0050	0.0277	0.4000	2.400
0.0125	0.0750	0.4500	2.700
0.0250	0.1500	0.5000	3.000
0.0500	0.3000	0.5500	3.300
0.0750	0.4500	0.6000	3.600
0.1000	0.6000	0.6500	3.900
0.1250	0.7500	0.7000	4.200
0.1500	0.9000	0.7500	4.500
0.1750	1.0500	0.8000	4.800
0.2000	1.2000	0.8500	5.100
0.2500	1.5000	0.9000	5.400
0.3000	1.8000	0.9500	5.700

Figure 3. Model Geometry.

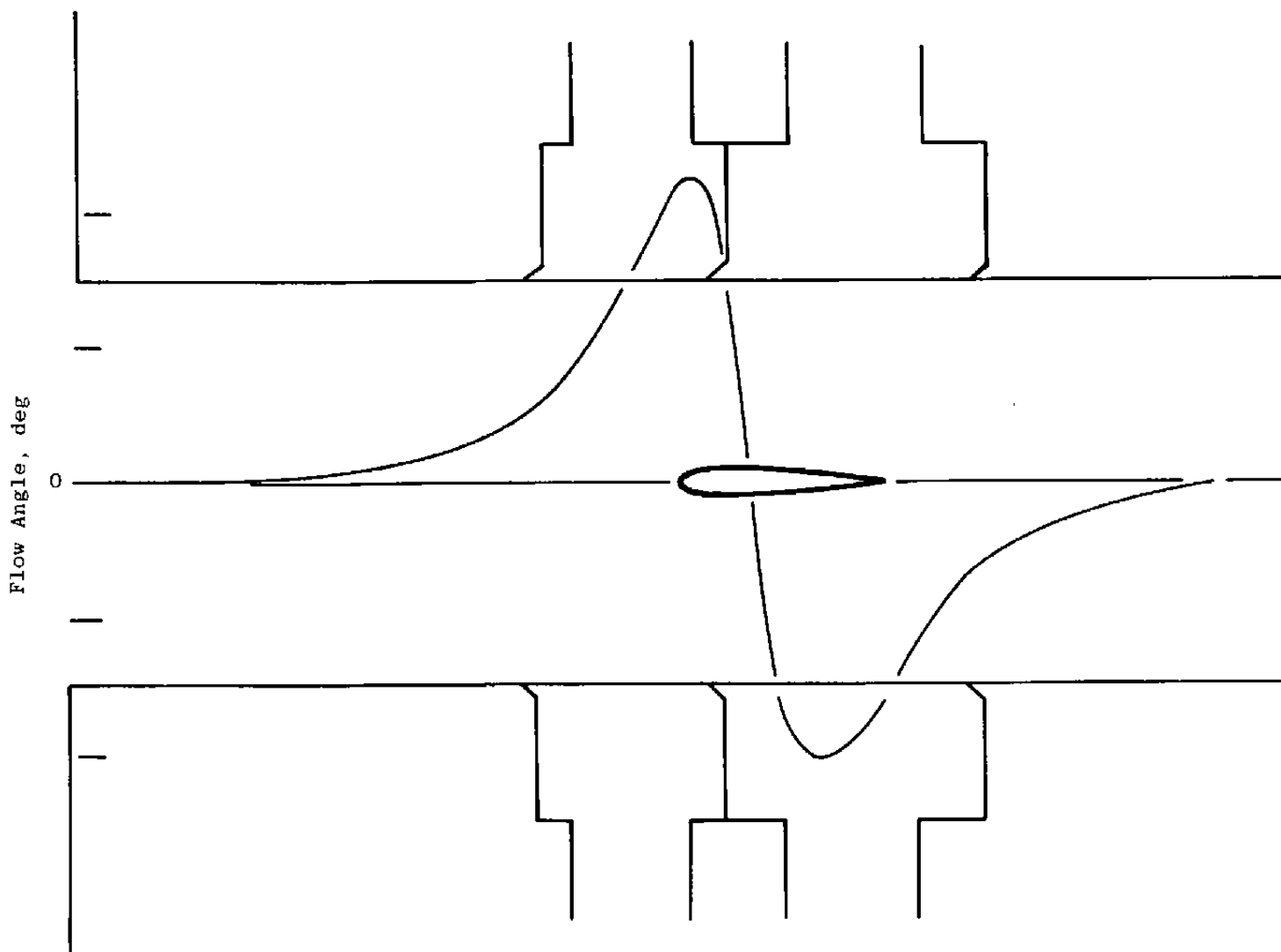


Figure 4. Experimental configuration: subplena location by flow-angle strategy.

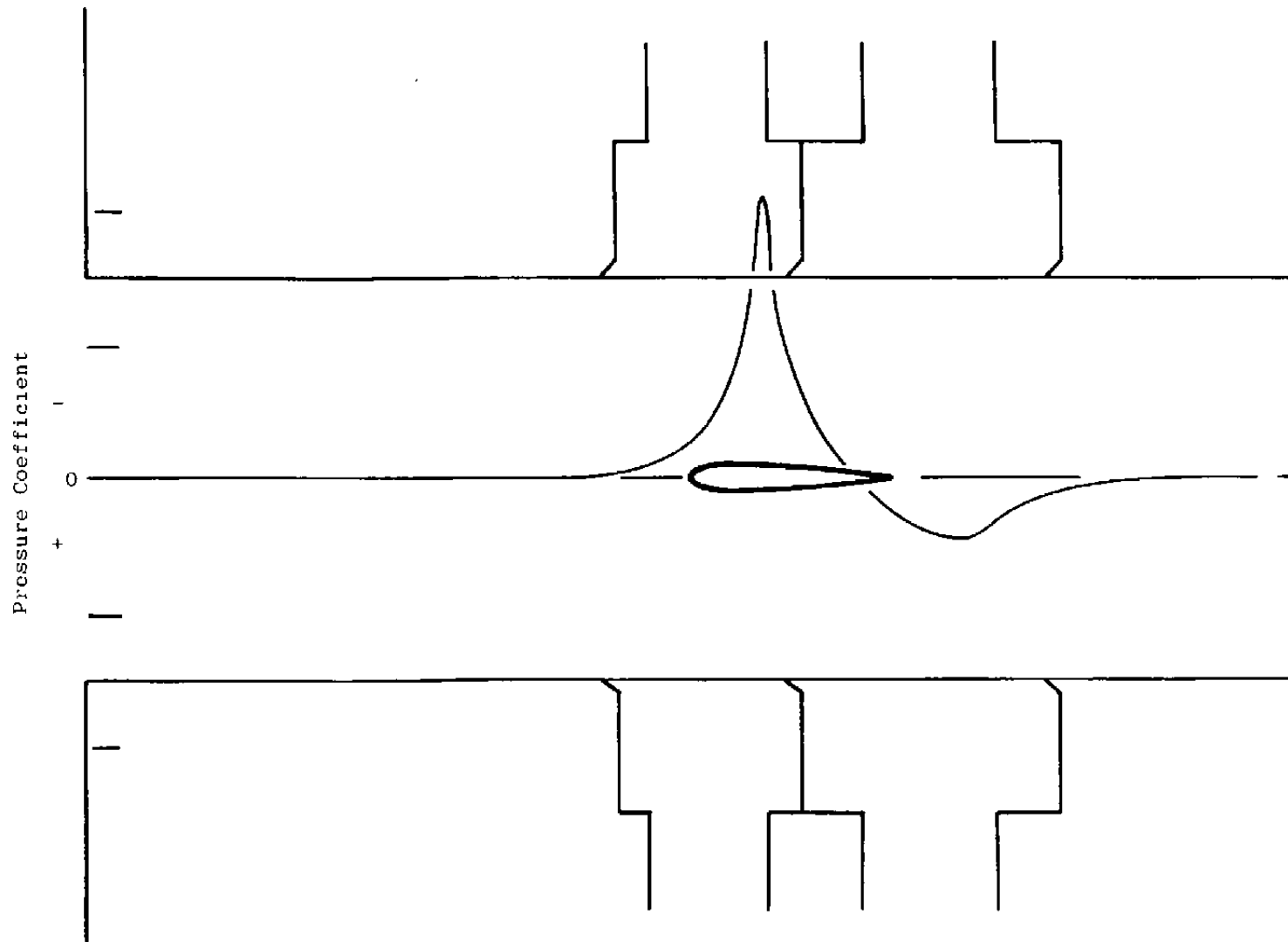


Figure 5. Experimental configuration 3: subplena location by pressure strategy.

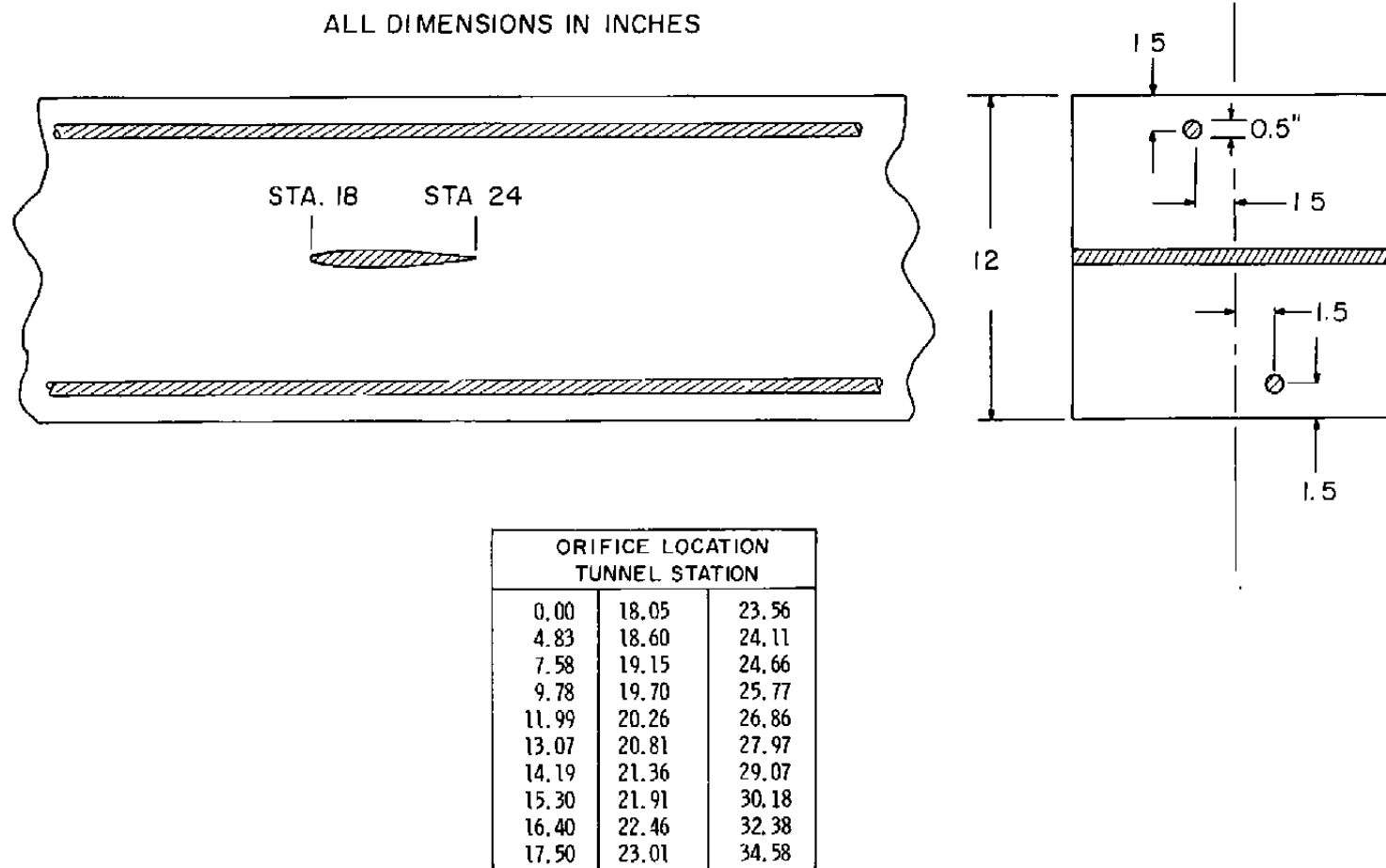
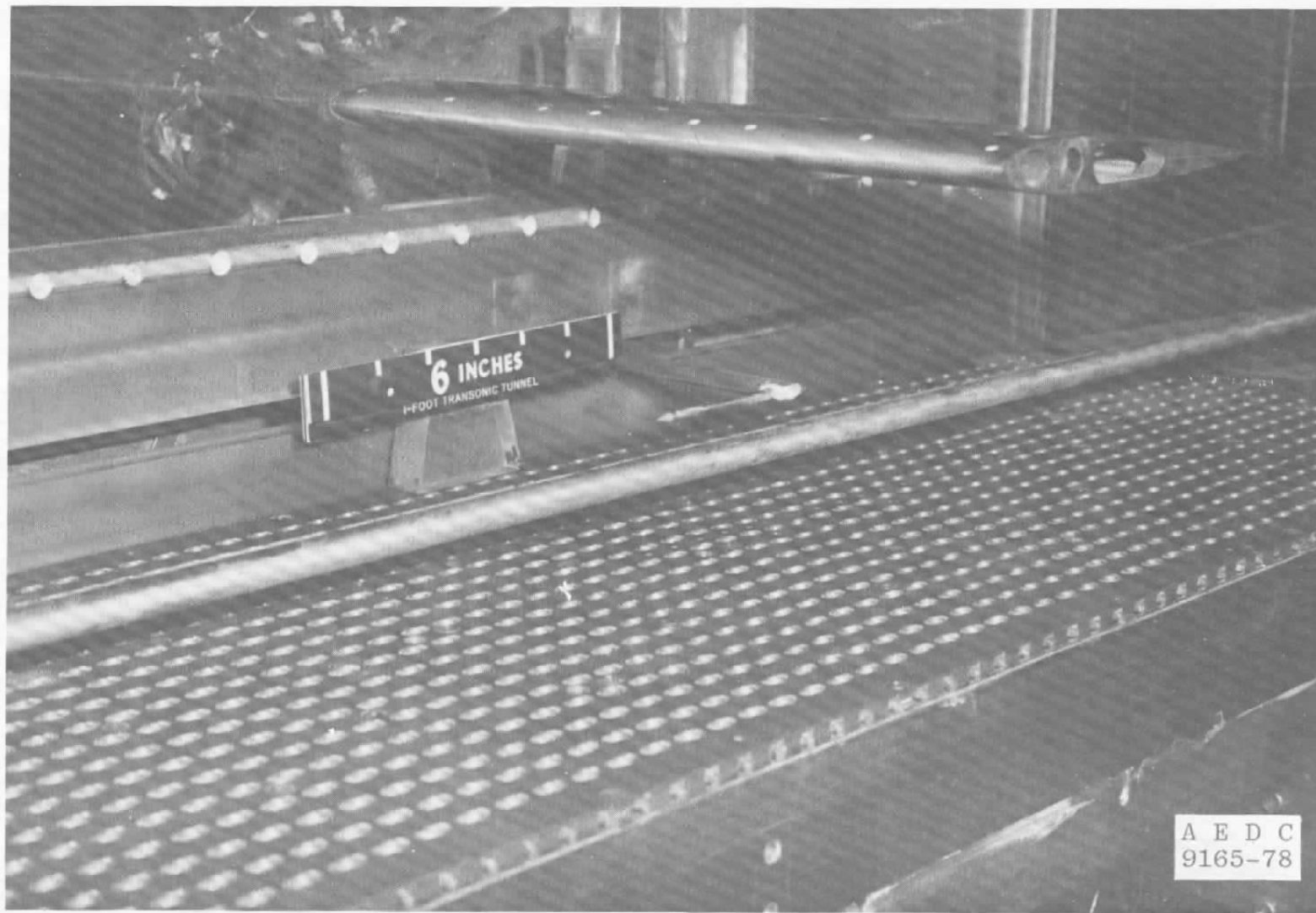
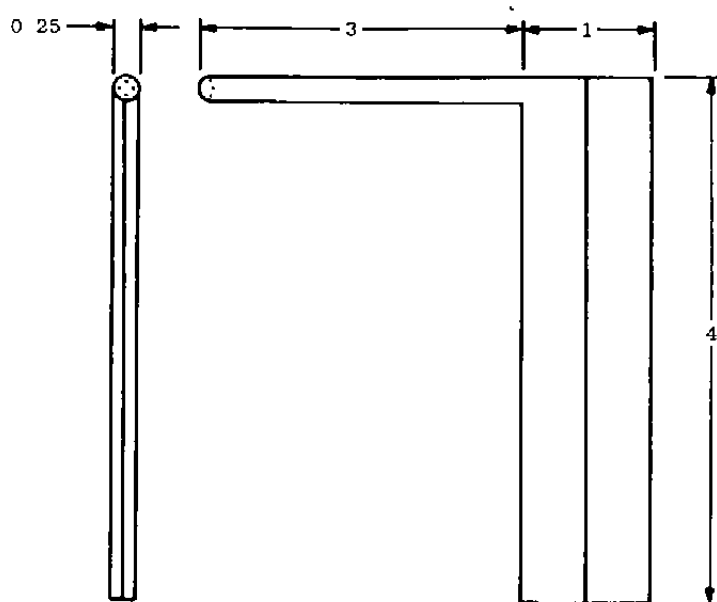


Figure 6. Static pressure pipe.

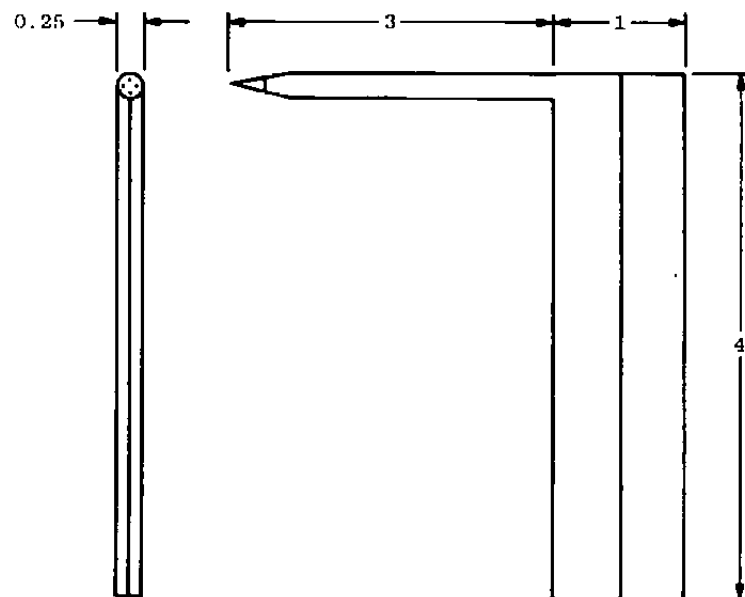


a. Test section arrangement
Figure 7. Flow-angle probe system and probe details.



Hemisphere Probe

All Dimensions in Inches



Cone Probe

b. Probe details

Figure 7. Concluded.

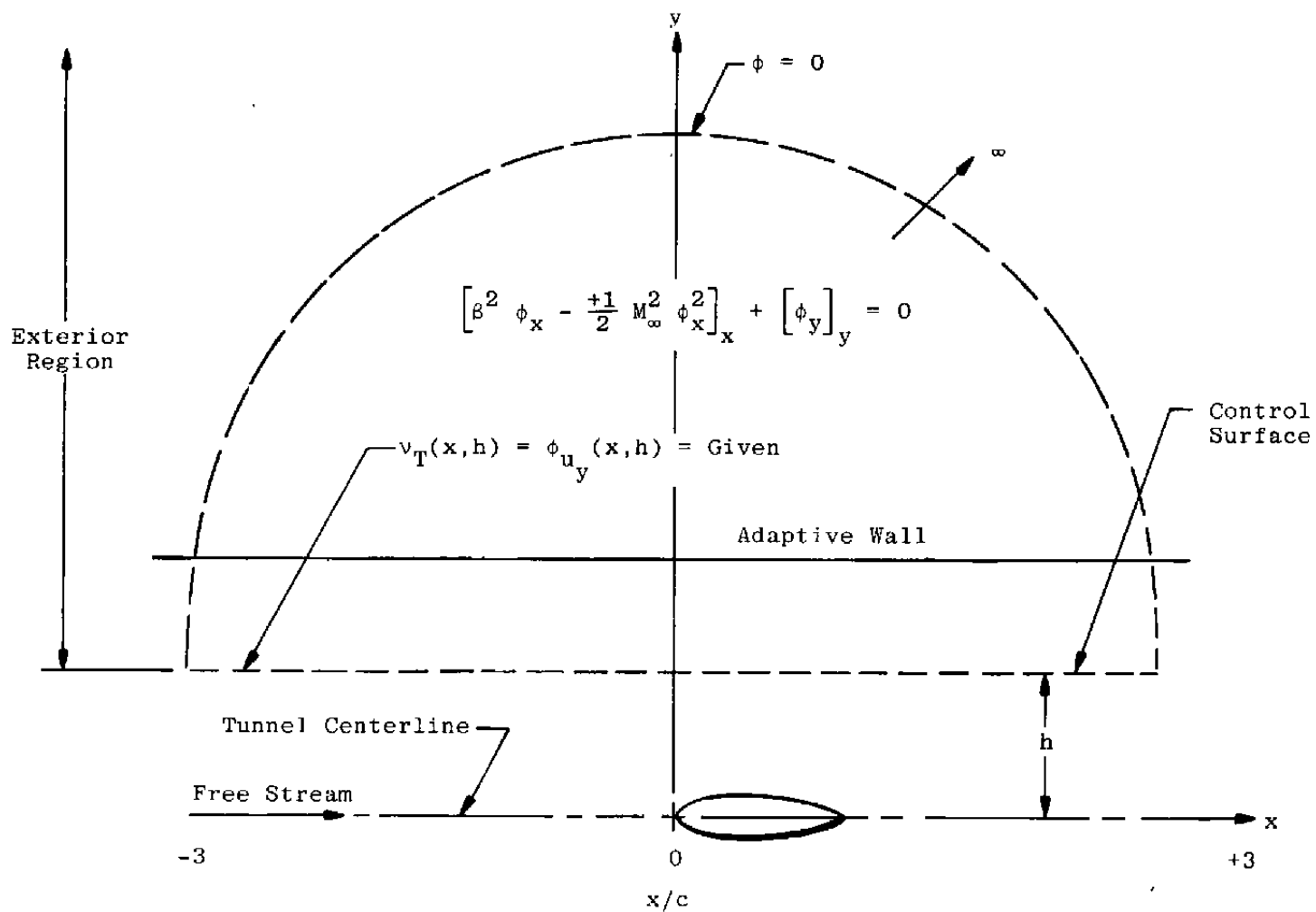


Figure 8. Boundary-value problem of exterior unconfined region.

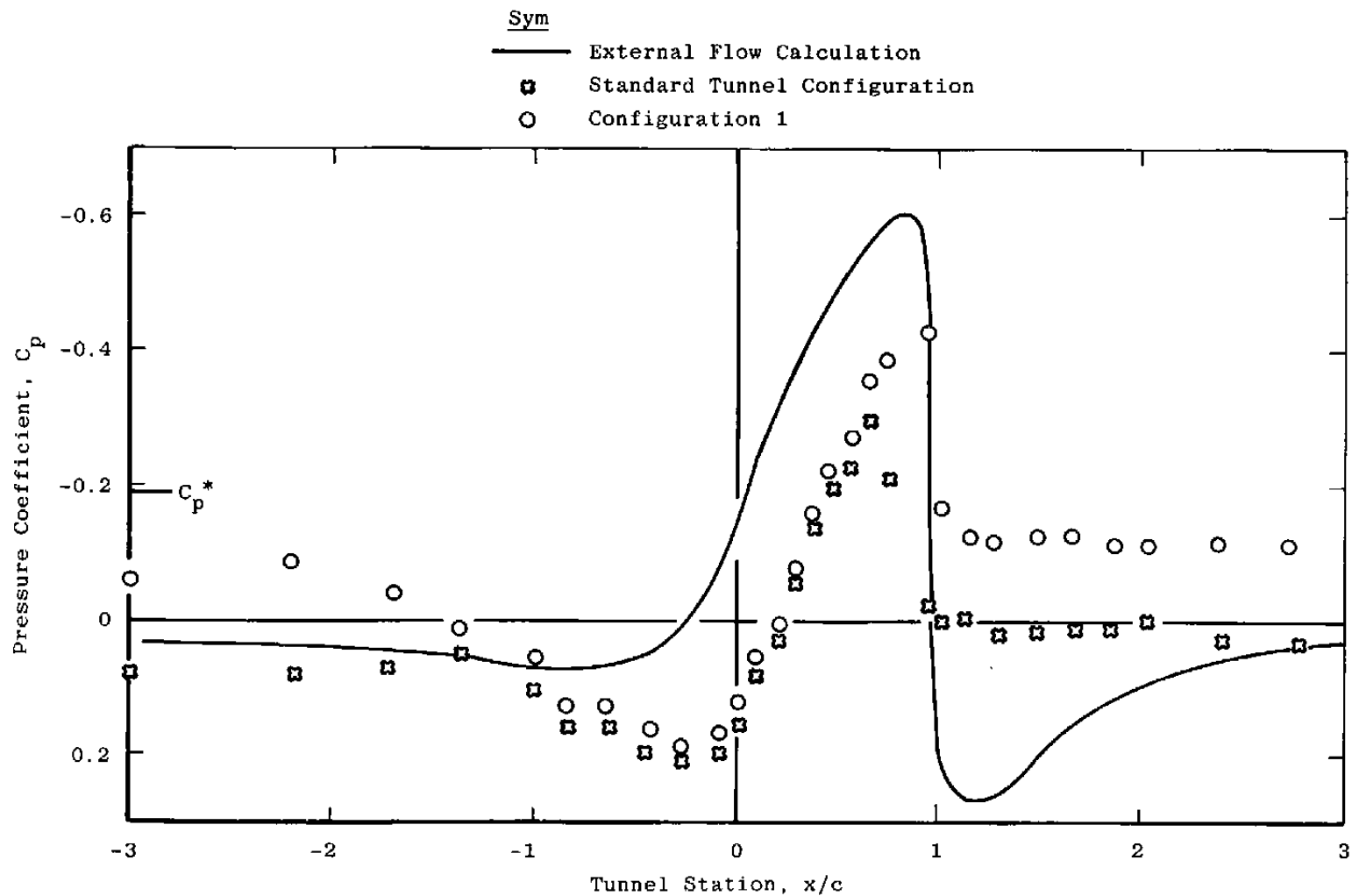


Figure 9. Control surface pressure distribution, $M_\infty = 0.9$ and $\alpha = 0$.

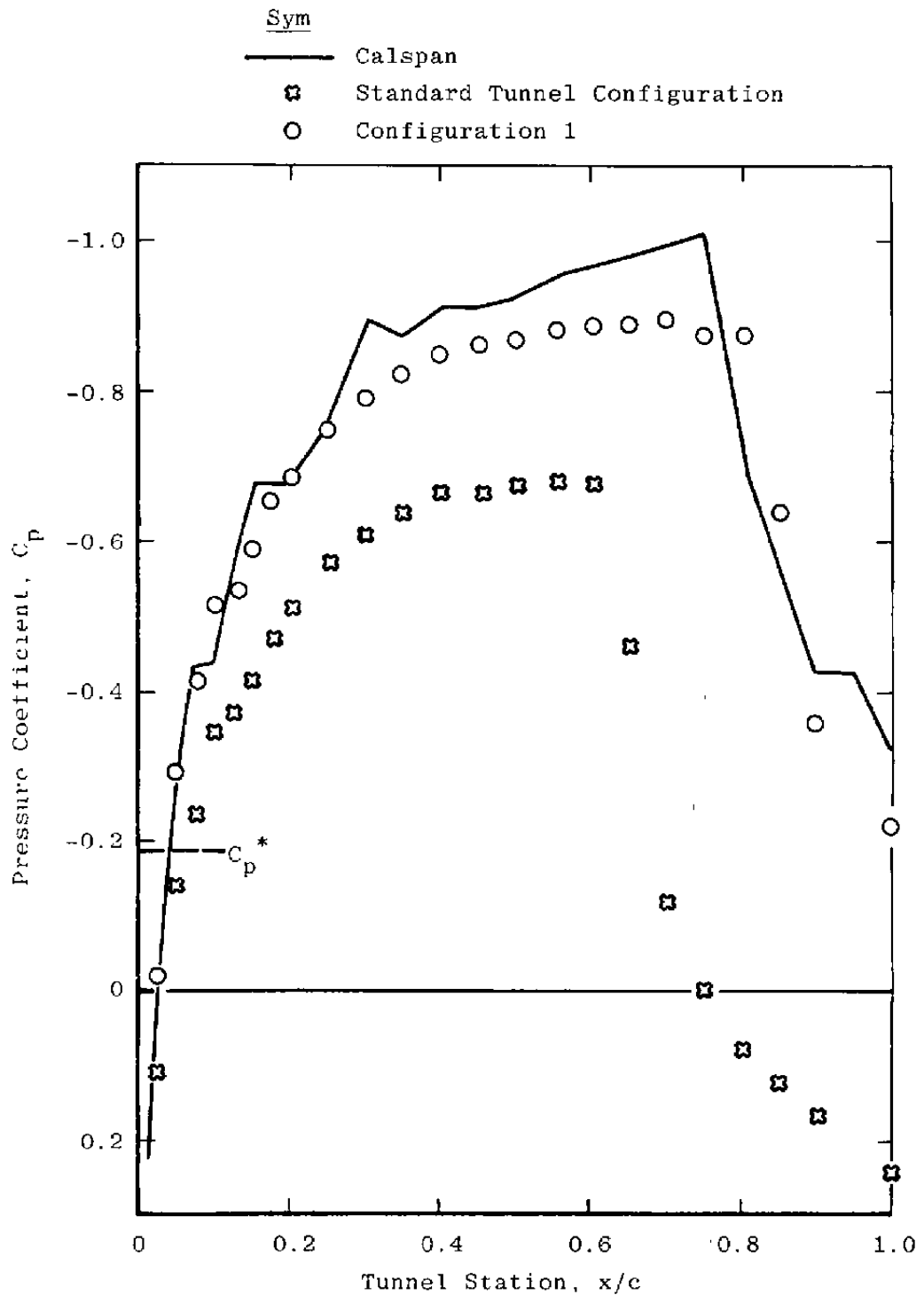


Figure 10. Model surface pressure distribution, $M_\infty = 0.9$ and $\alpha = 0$.

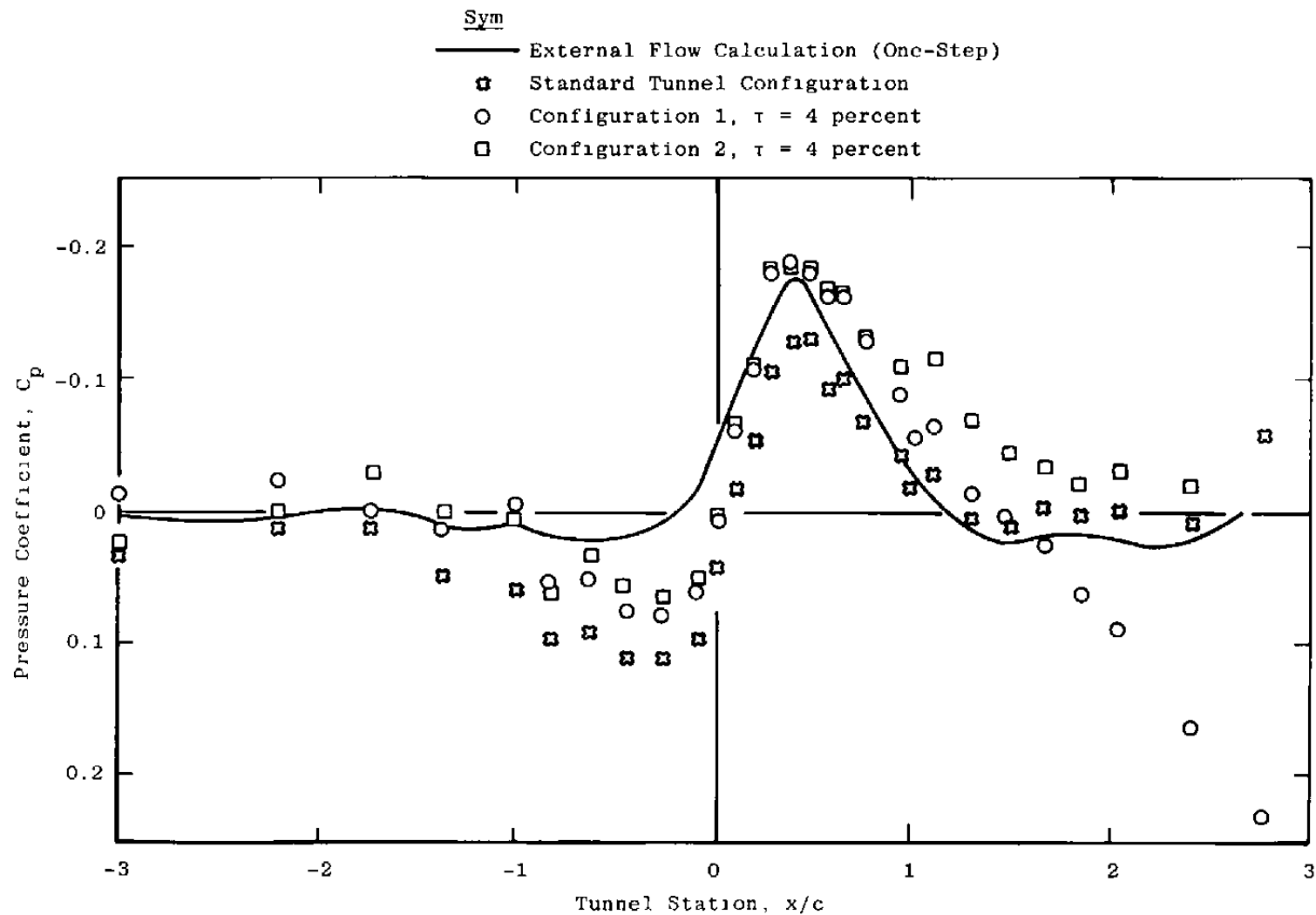


Figure 11. Control surface pressure distribution, $M_\infty = 0.8$ and $\alpha = 0$.

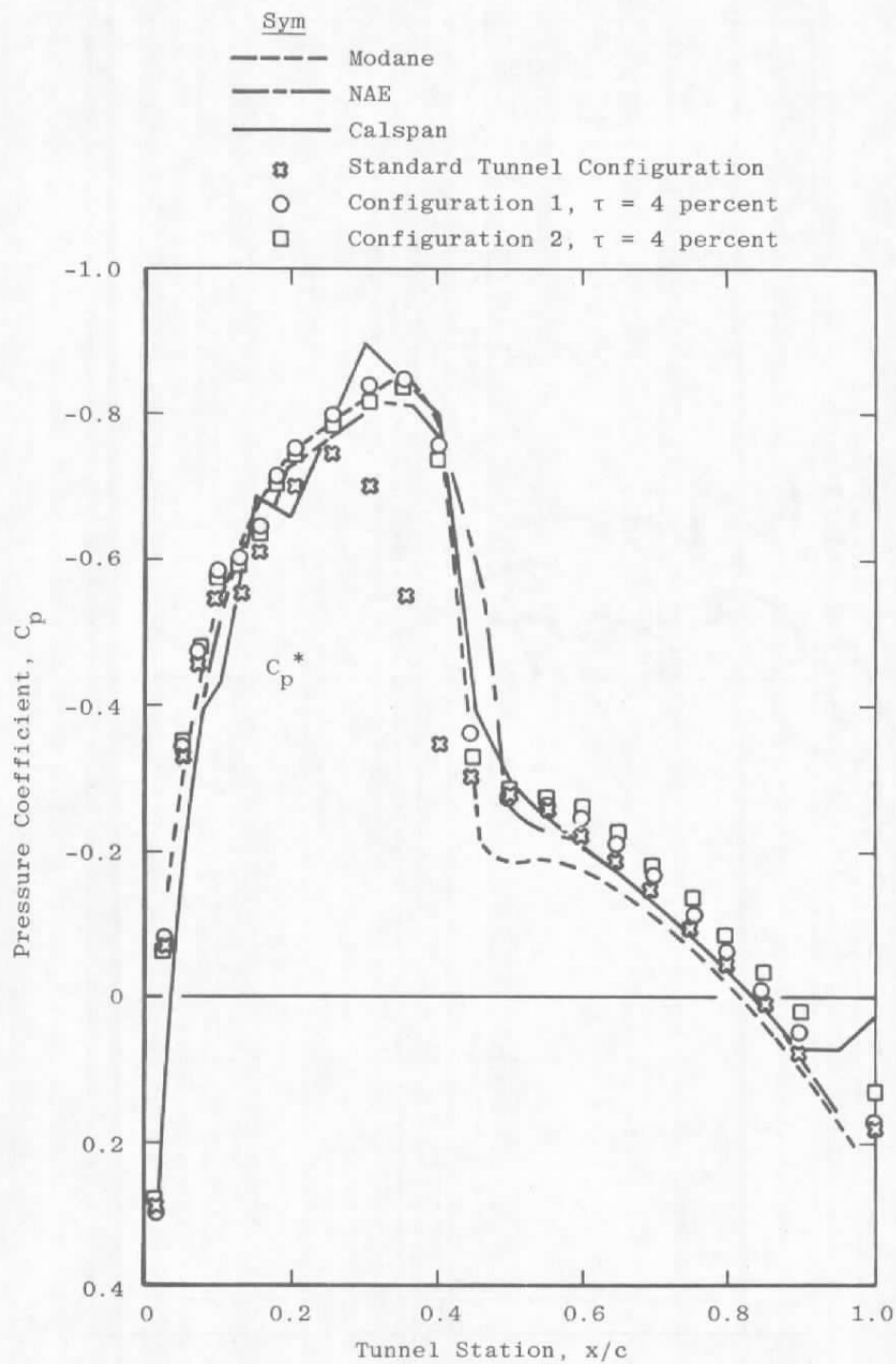


Figure 12. Model surface pressure distribution, $M_\infty = 0.8$ and $\alpha = 0$.

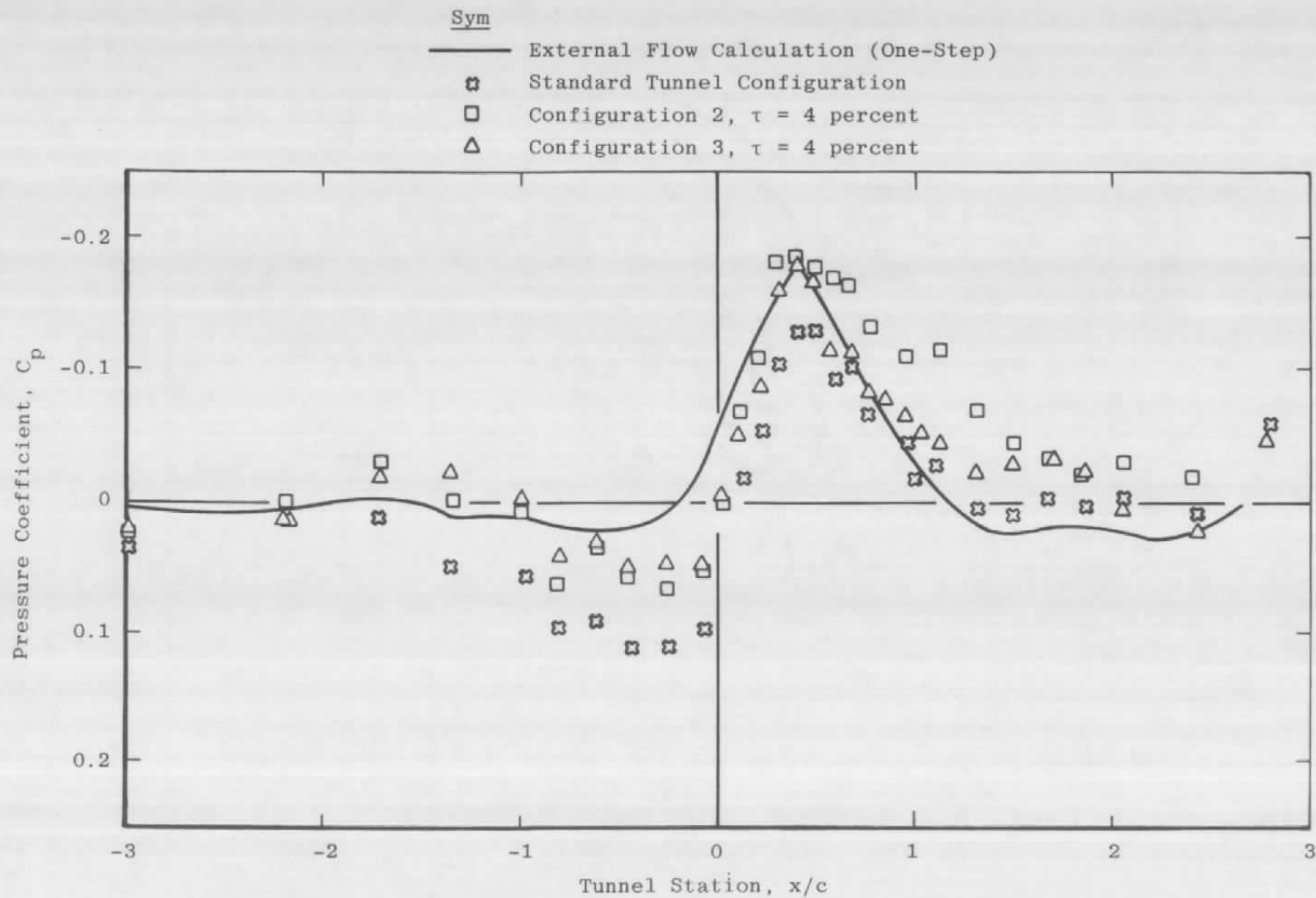


Figure 13. Control surface pressure distribution, $M_\infty = 0.8$
and $\alpha = 0$.

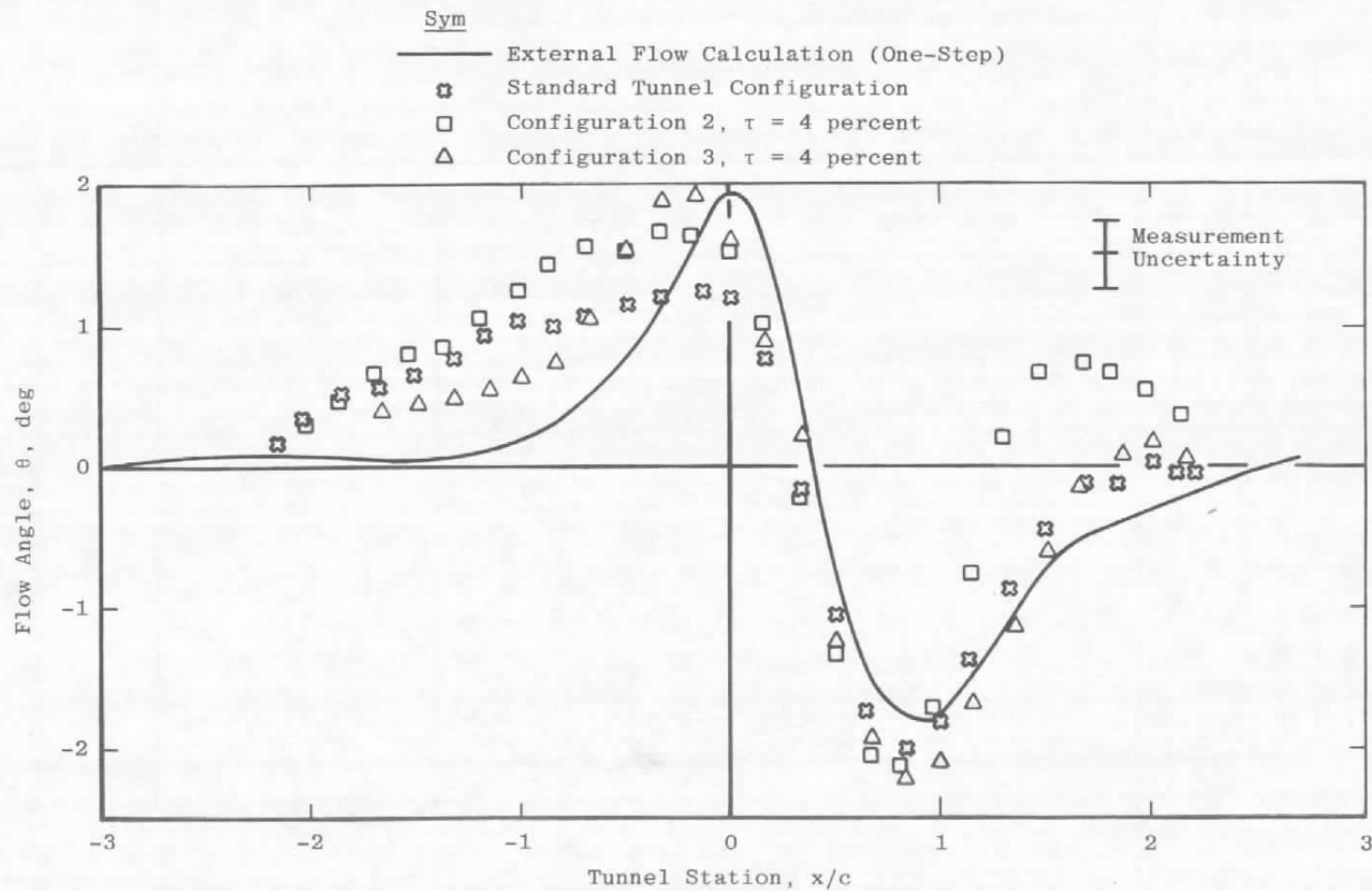


Figure 14. Upper control surface flow-angle distribution, $M_\infty = 0.8$ and $\alpha = 0$.

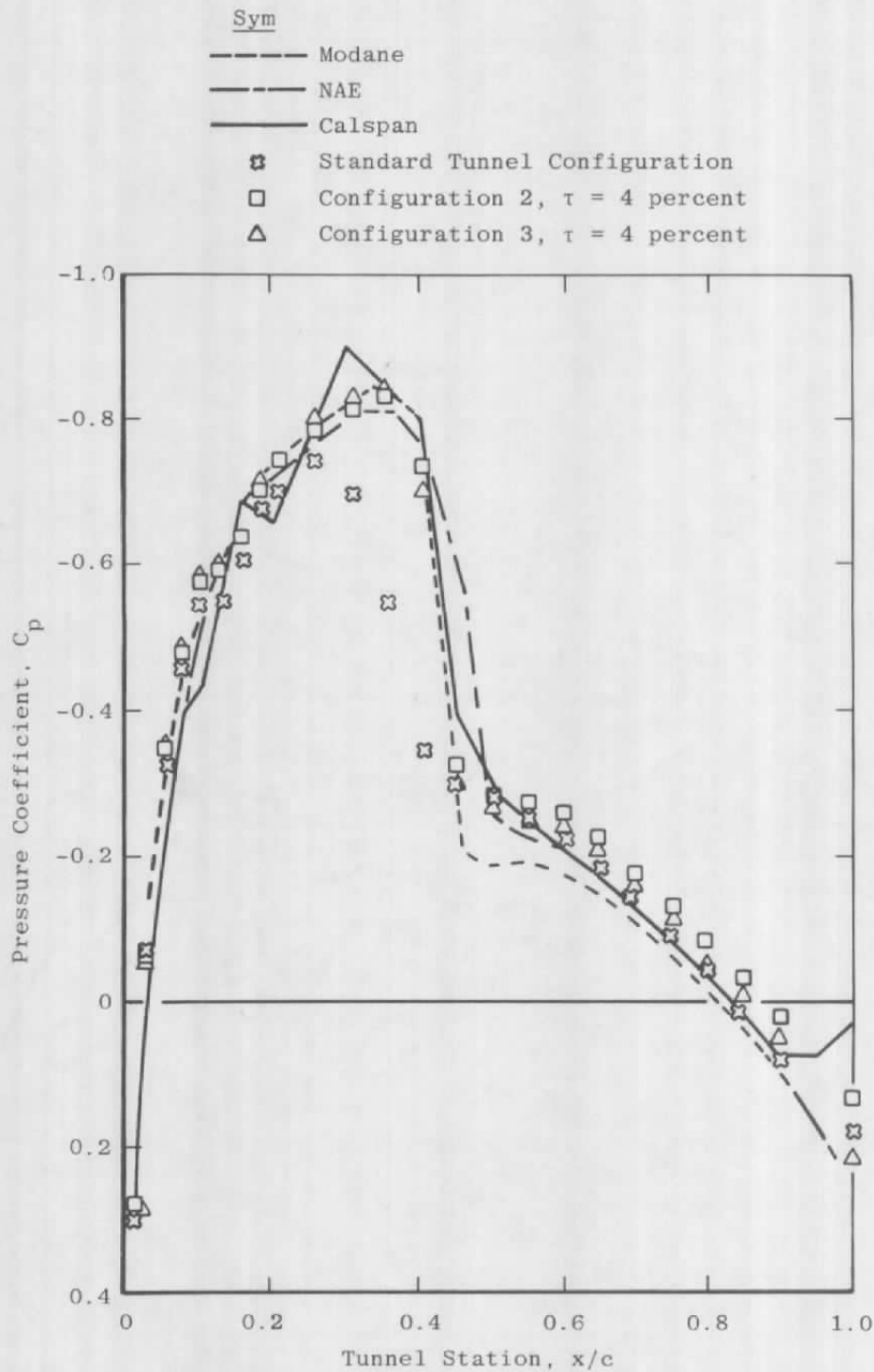


Figure 15. Model surface pressure distribution, $M_\infty = 0.8$ and $\alpha = 0$.

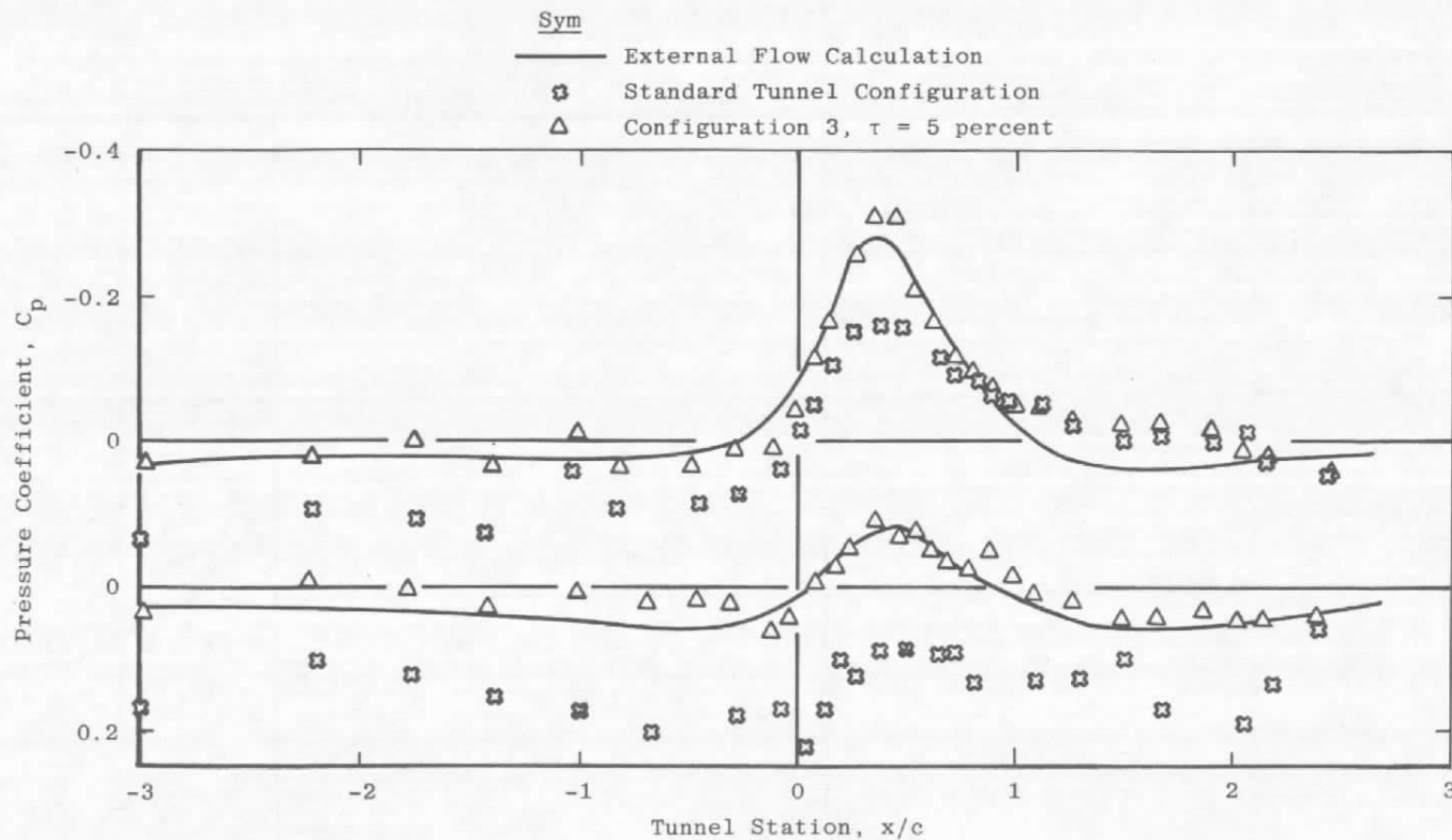
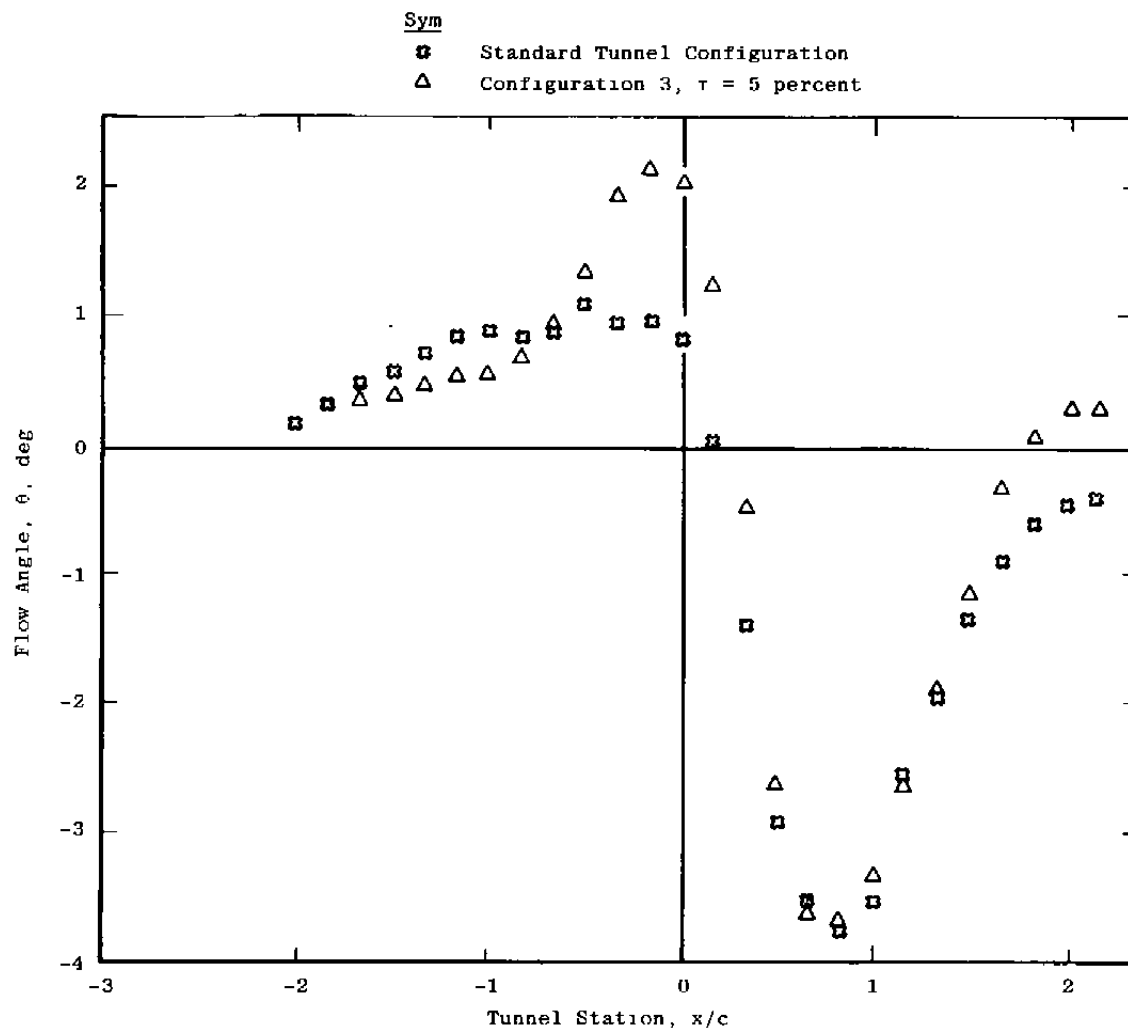
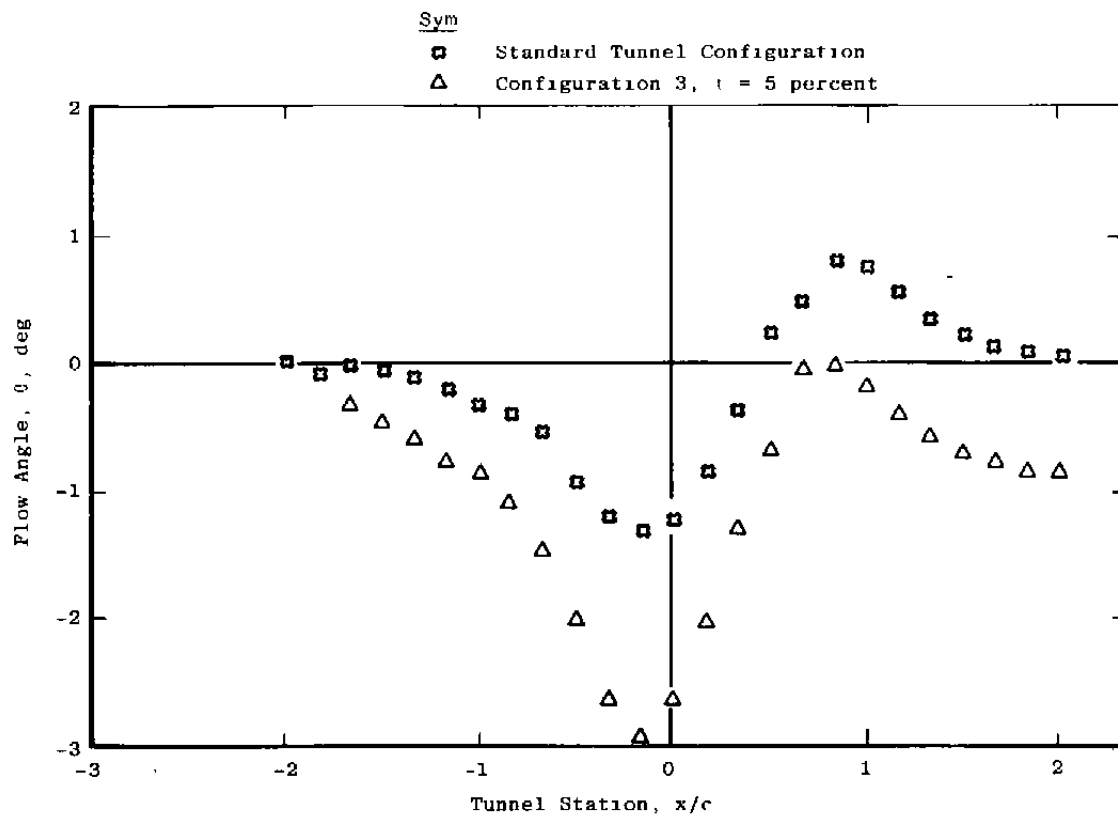


Figure 16. Control surface pressure distribution, $M_\infty = 0.8$
 and $\alpha = 0$.



a. Upper surface

Figure 17. Control surface flow-angle distribution, $M_\infty = 0.8$ and $\alpha = 2$.



b. Lower control surface

Figure 17. Concluded.

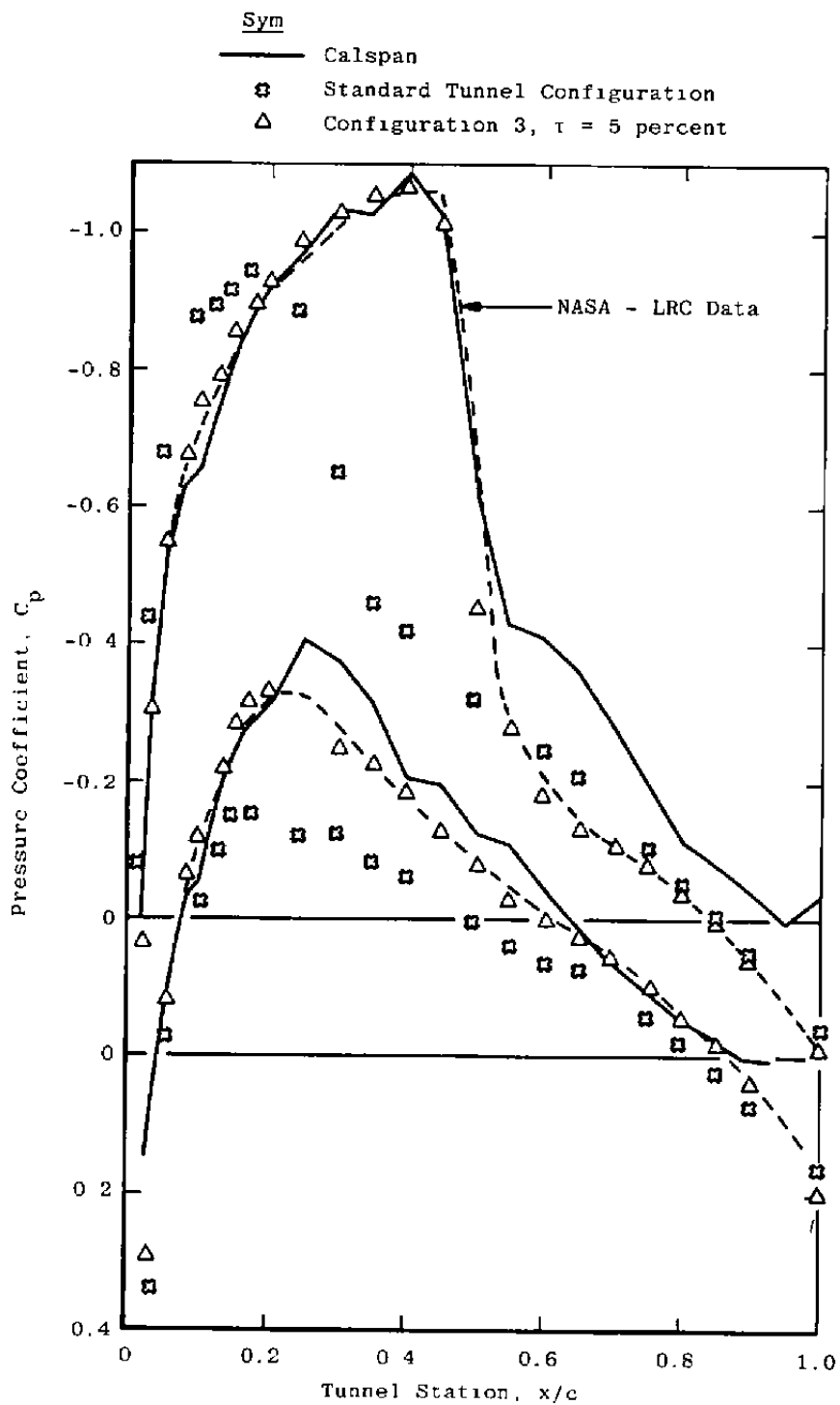


Figure 18. Model surface pressure distribution, $M_\infty = 0.8$
and $\alpha = 2$.

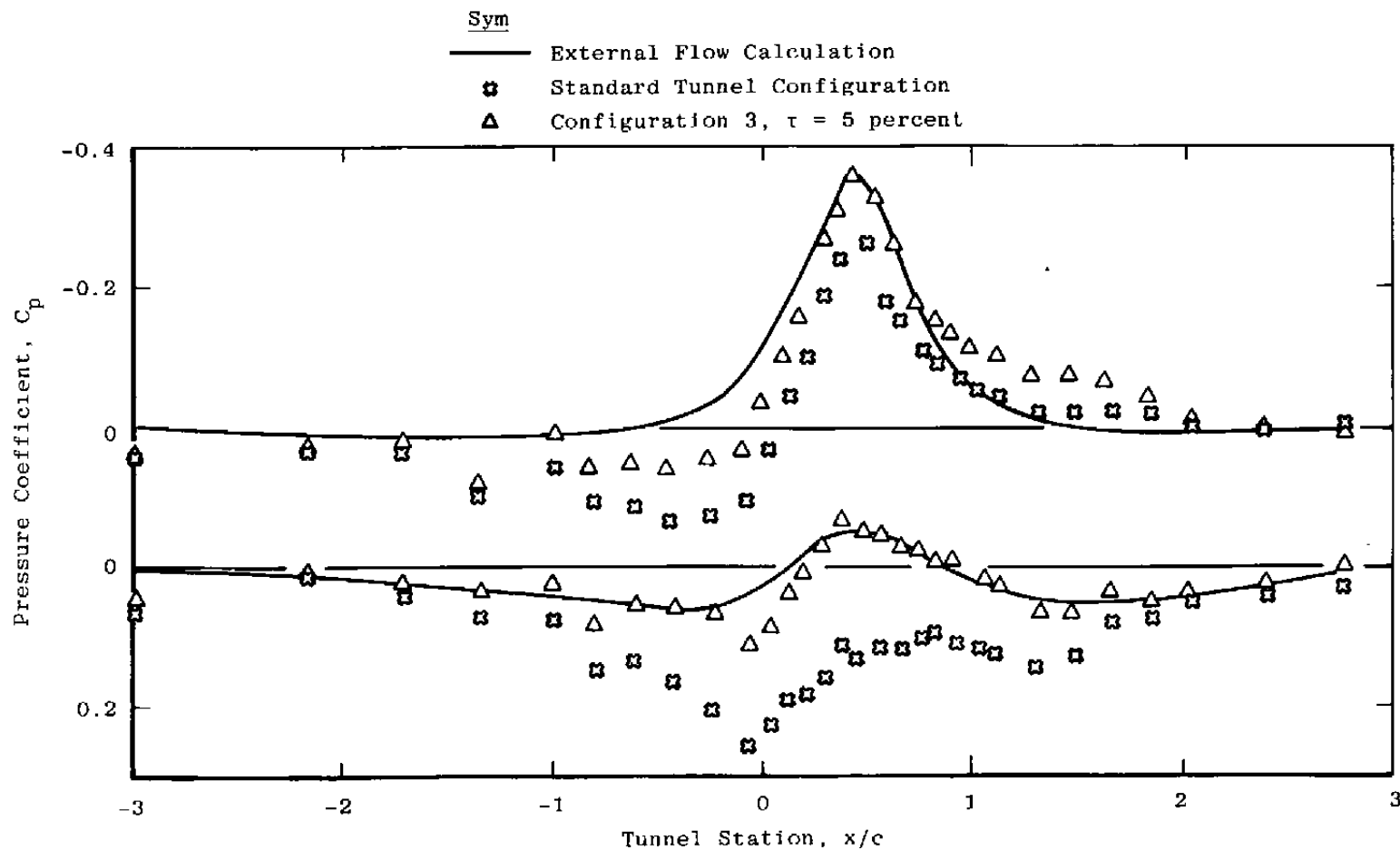
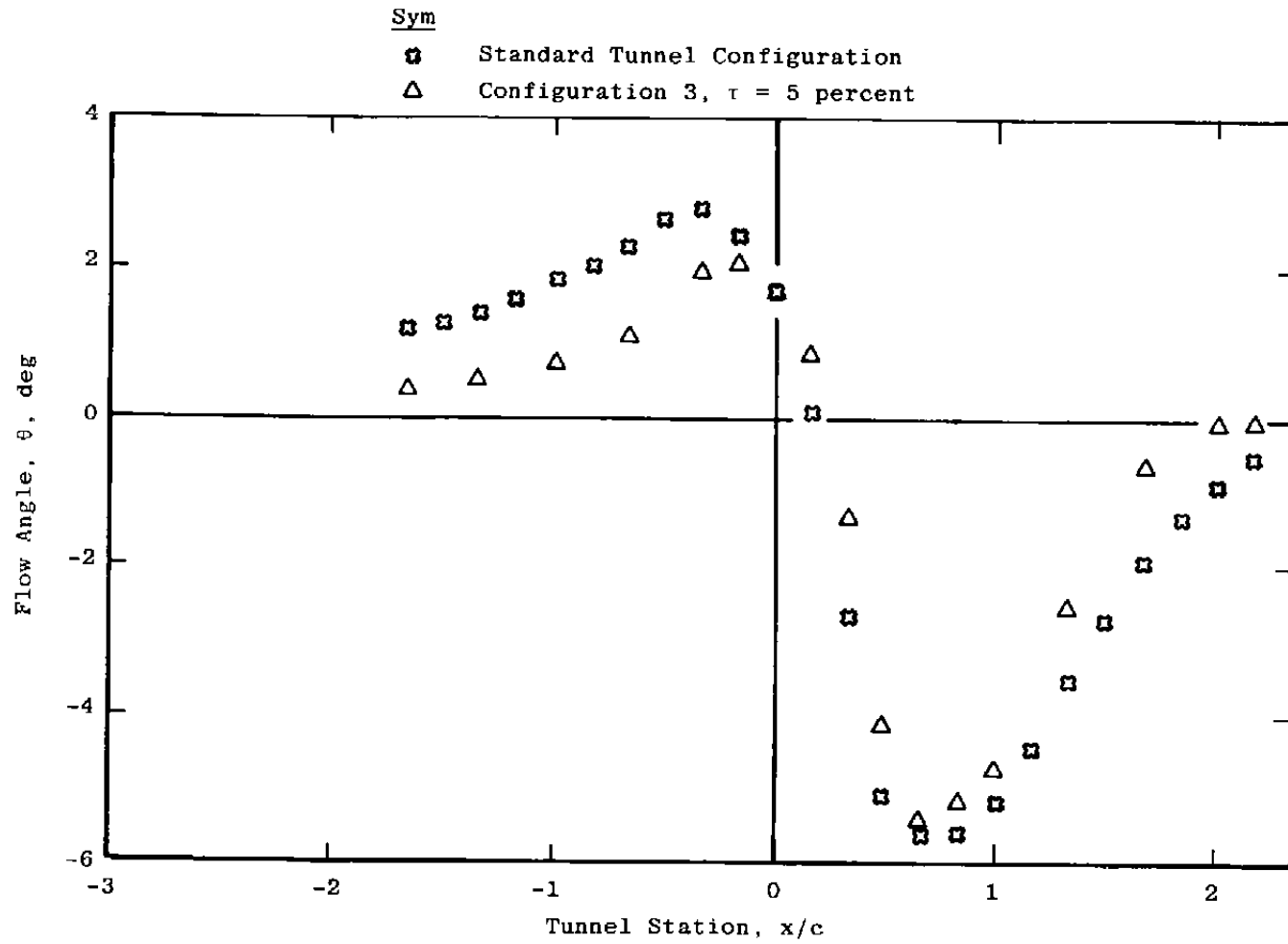
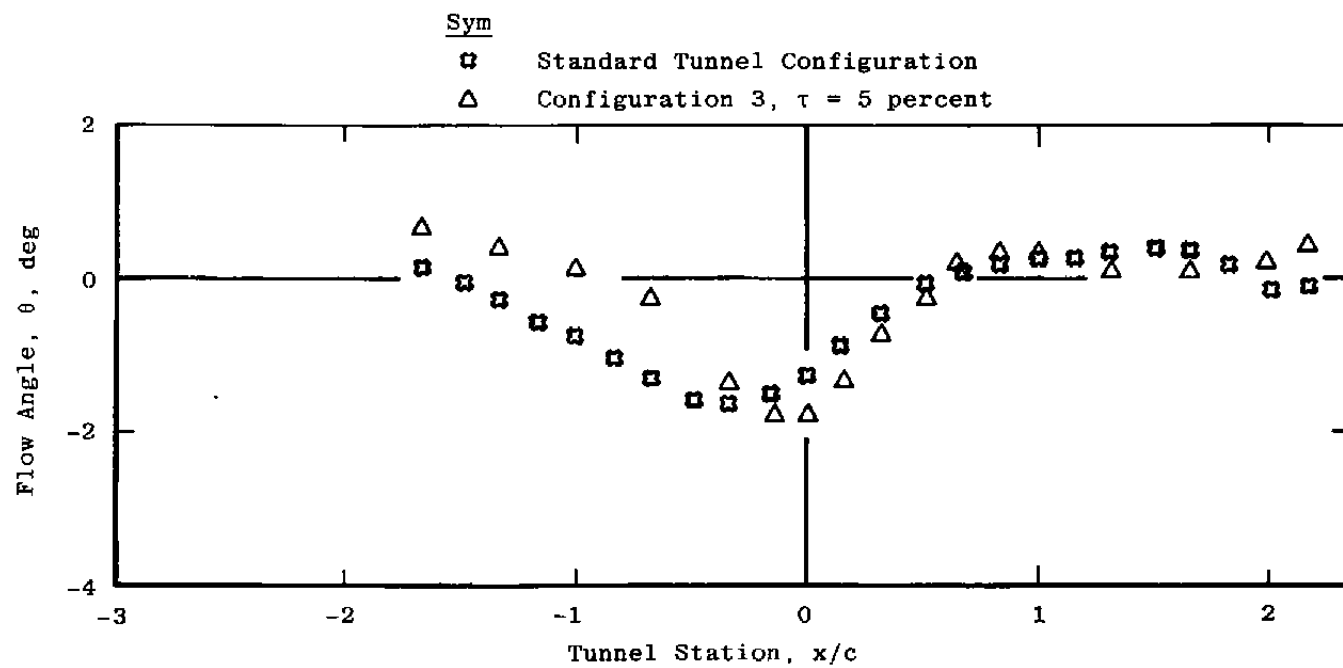


Figure 19. Control surface pressure distribution, $M_\infty = 0.8$
 and $\alpha = 4$.



a. Upper control surface

Figure 20. Control surface flow-angle distribution, $M_\infty = 0.8$ and $\alpha = 4$.



b. Lower control surface
Figure 20. Concluded.

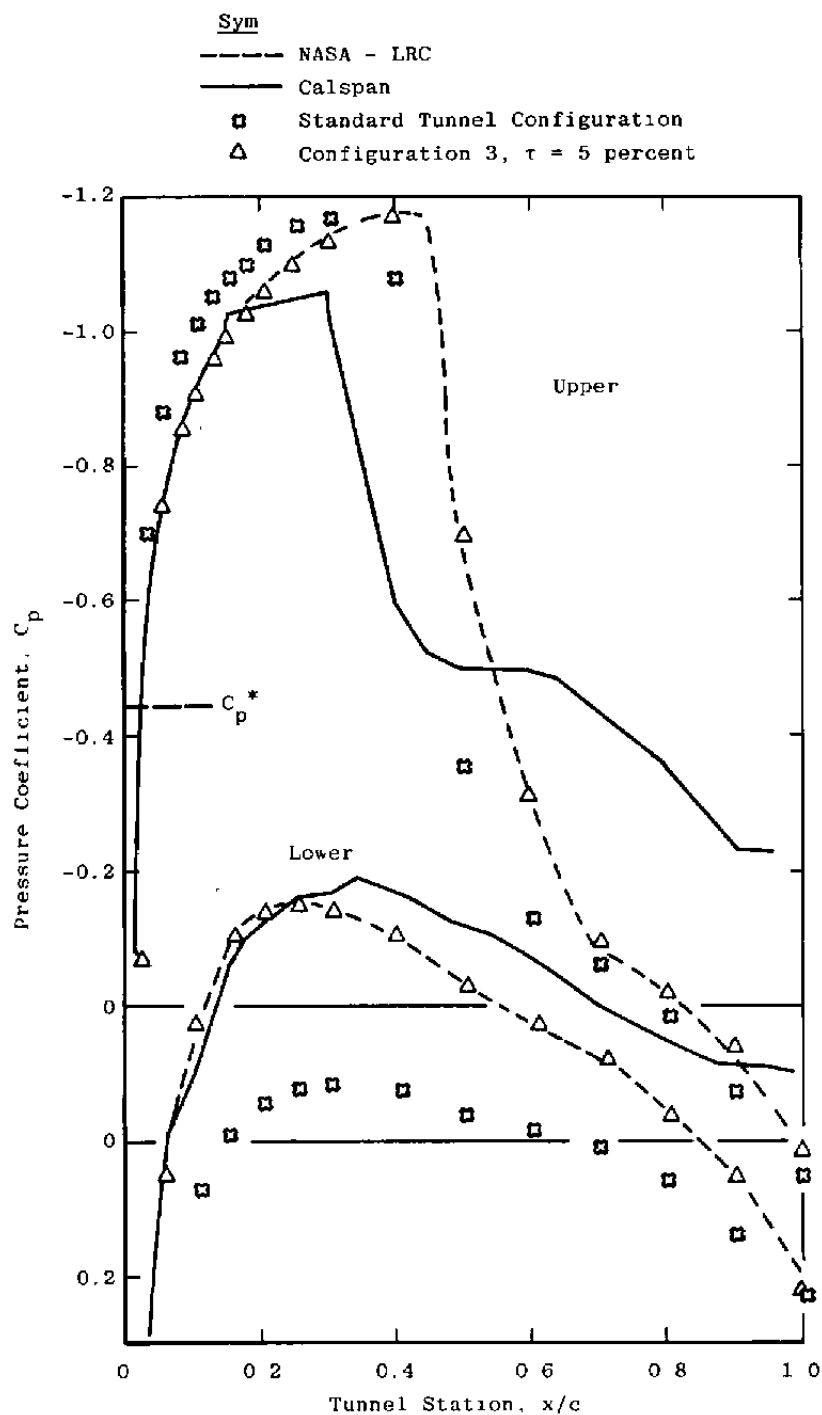


Figure 21. Model surface pressure distribution, $M_\infty = 0.8$ and $\alpha = 4^\circ$.

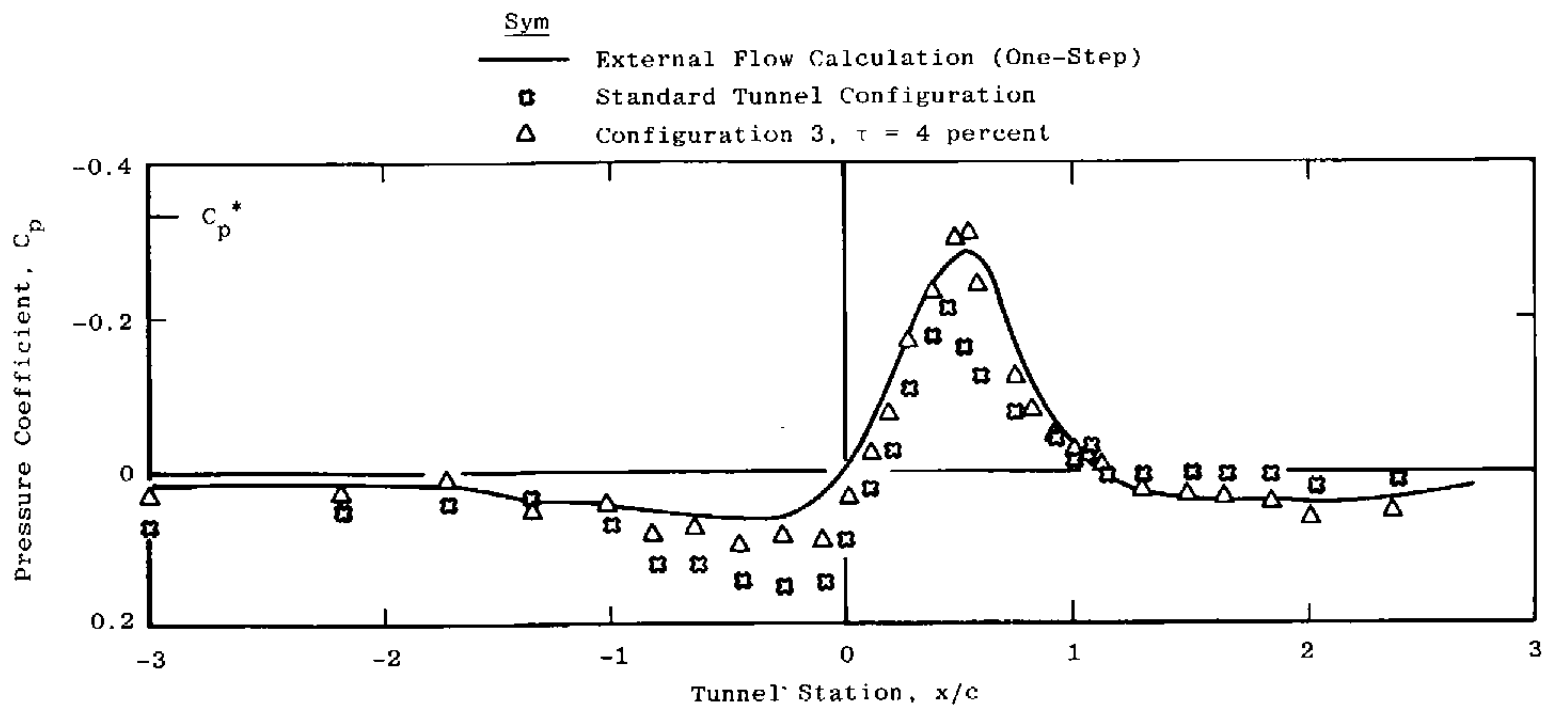


Figure 22. Control surface pressure distribution, $M_\infty = 0.8$
 and $\alpha = 0$.

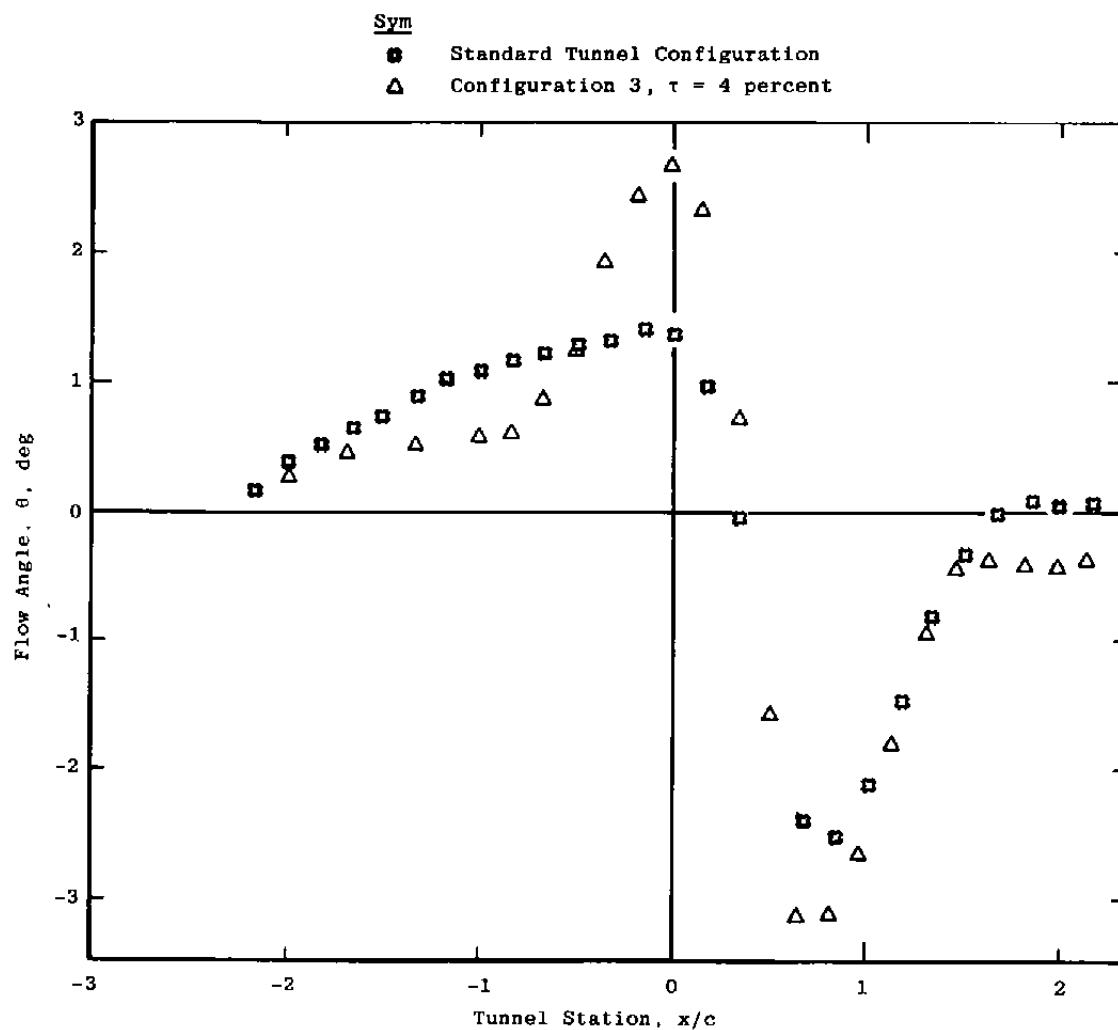


Figure 23. Upper control surface flow-angle distribution, $M_\infty = 0.85$ and $\alpha = 0$.

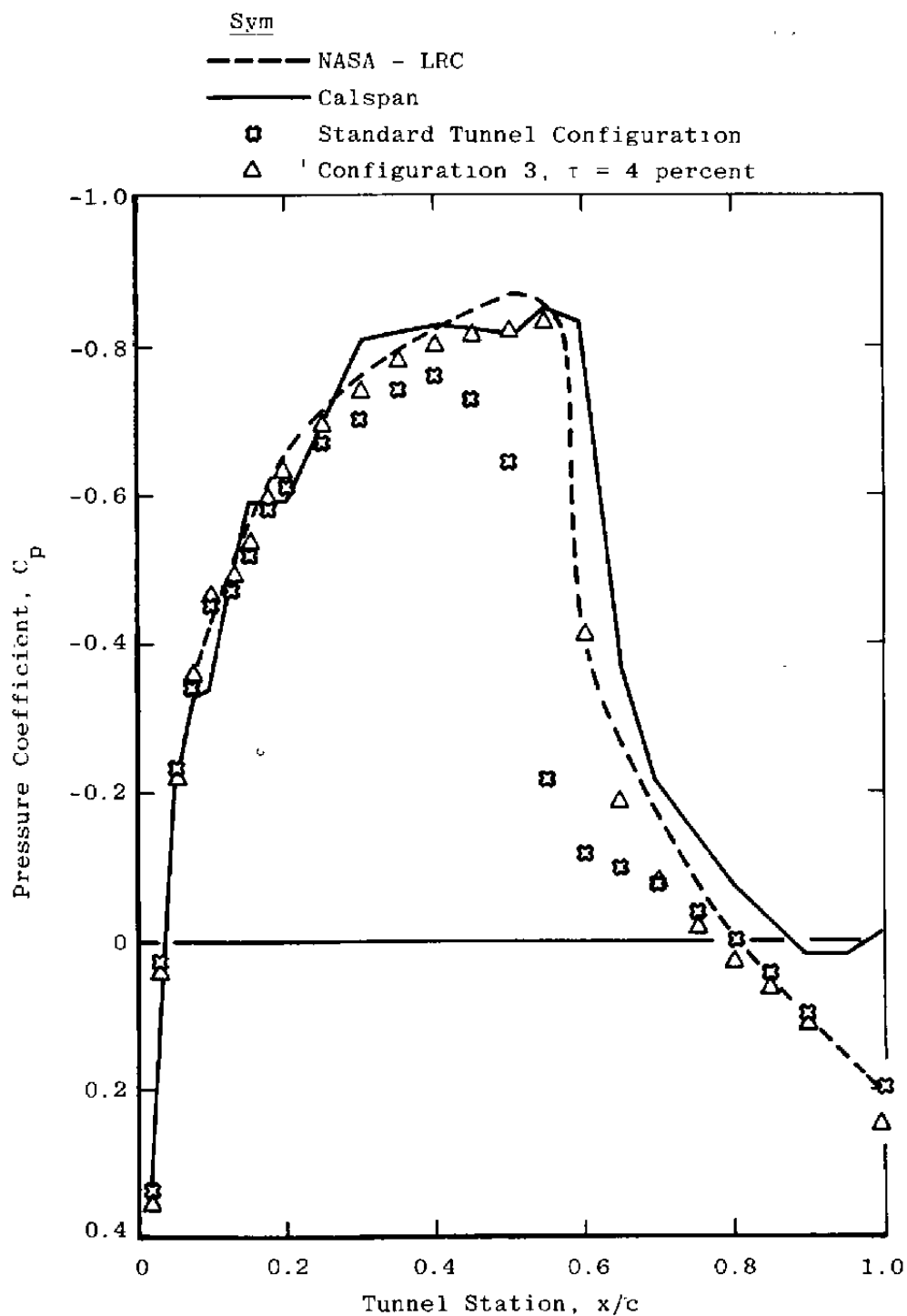


Figure 24. Model surface pressure distribution, $M_\infty = 0.85$ and $\alpha = 0$.

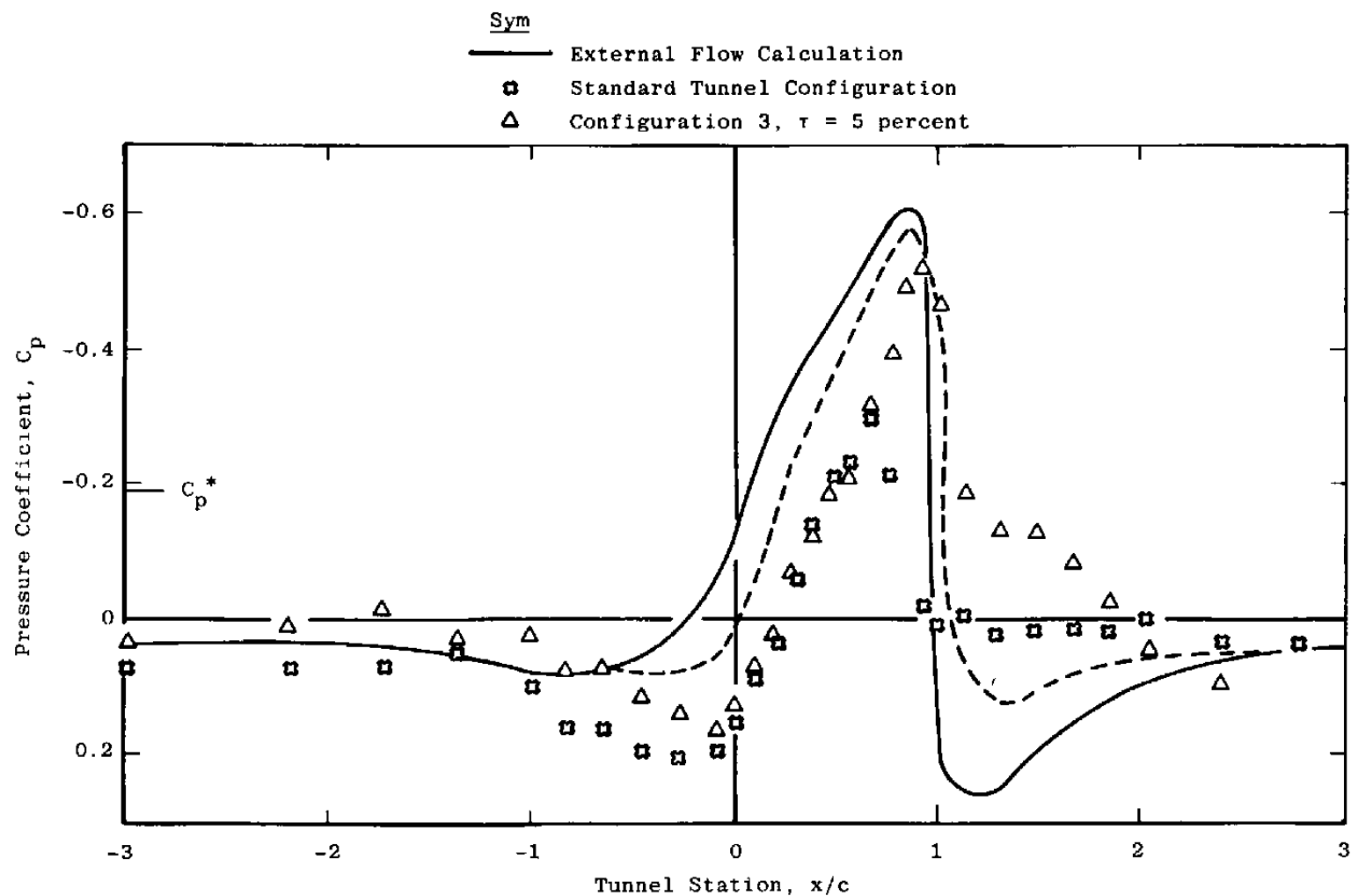


Figure 25. Control surface pressure distribution, $M_\infty = 0.9$
 and $\alpha = 0$.

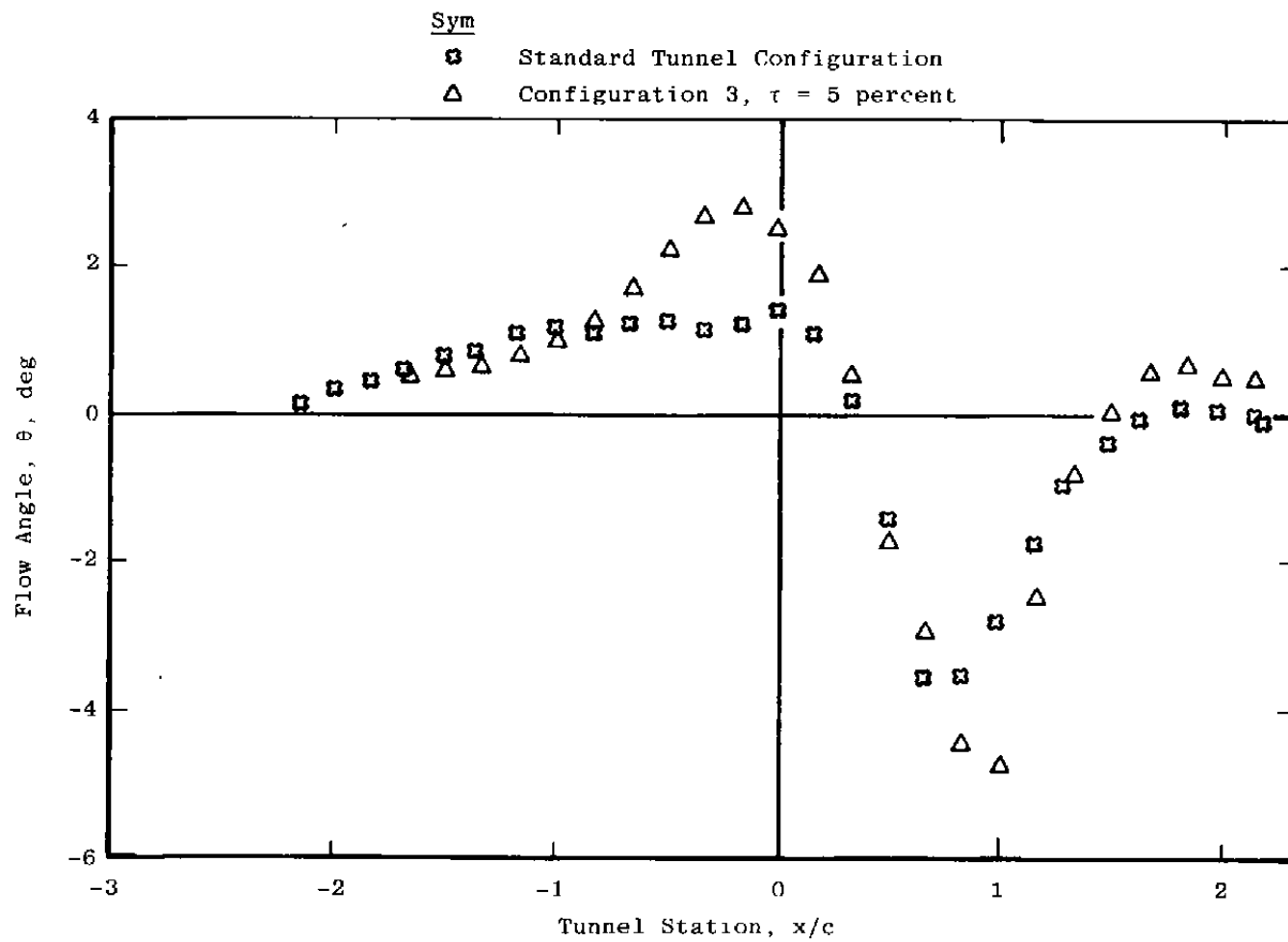


Figure 26. Upper control surface flow-angle distribution, $M_\infty = 0.9$ and $\alpha = 0$.

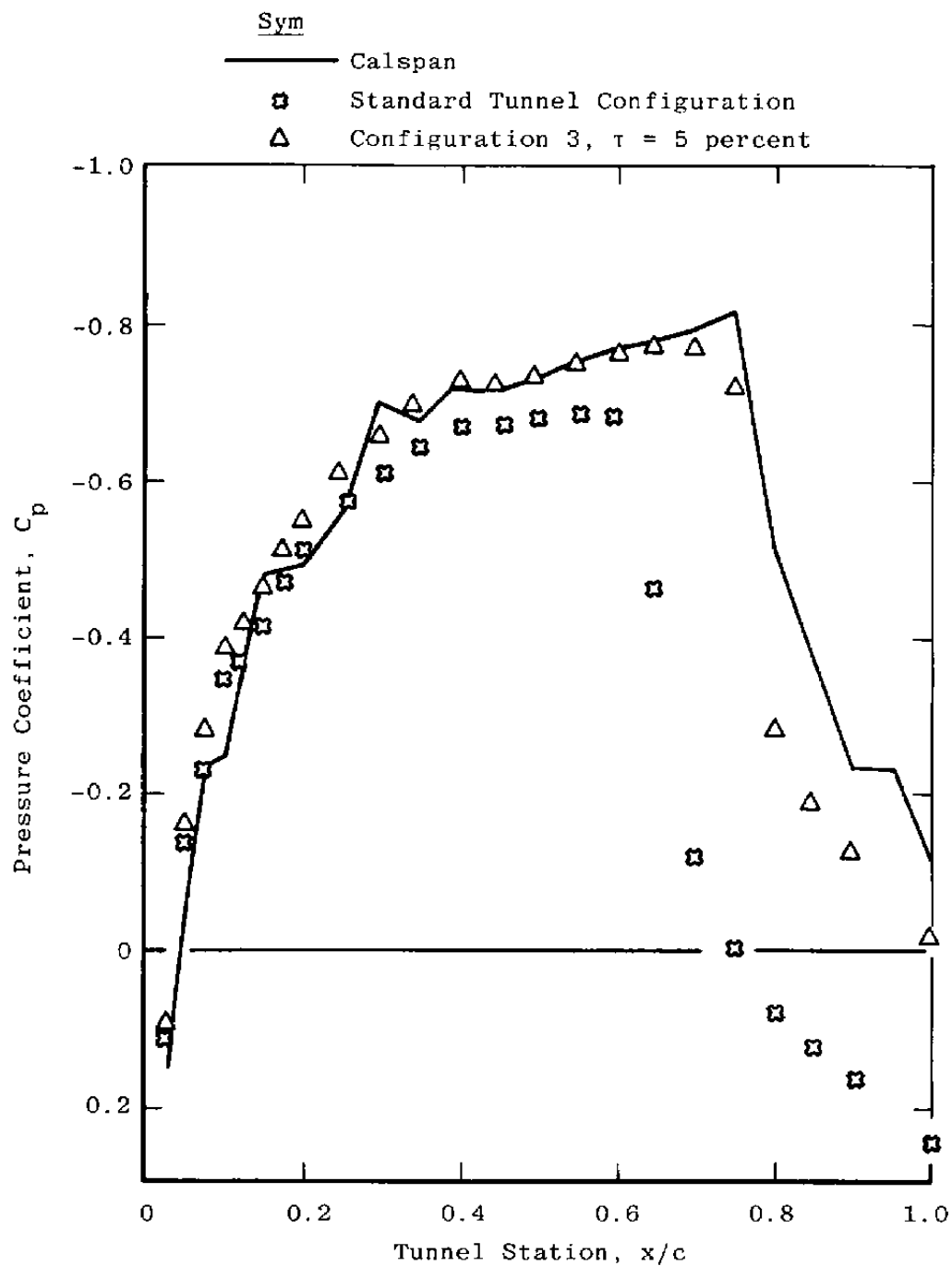


Figure 27. Model surface pressure distribution, $M_\infty = 0.9$
and $\alpha = 0$.

Table 1. Pertinent Test Data Information

Source	Facility	Model Chord, in.	Reynolds Number Based on Chord
Calspan	8-ft Transonic Wind Tunnel	6	10^6
NASA-LRC	8-ft 2-D Transonic Wind Tunnel	25	3×10^6
NAE	5-ft Trisonic Wind Tunnel	11.8	25×10^6
Modane	S3 (2.56 by a.84 ft)	8.3	4×10^6
AEDC	1-ft Transonic Wind Tunnel (Adaptive- Wall Test Section)	6	2.5×10^6

NOMENCLATURE

c	Chord
C_n	Pressure coefficient, $(p-p_{\infty}/q_{\infty})$
F	Degrees Fahrenheit
h	Control surface location
k	Relaxation factor
M_∞	Free-stream Mach number
p	Local static pressure, psf
p_∞	Free-stream static pressure, psf
P_c	Plenum chamber pressure, psf
P_T	Total tunnel pressure, psf
q_∞	Free-stream dynamic pressure, psf
R_e	Reynolds number
S	Control surface interface interior/exterior region
T_o	Stagnation temperature
t	Thickness ratio, y/c
u	Nondimensional streamwise component of disturbance velocity
u_∞	Nondimensional streamwise component of disturbance velocity given by one-step formula
v	Nondimensional normal component of disturbance velocity
X	Streamwise coordinate
x	Axial airfoil coordinate
x/c	Nondimensional streamwise airfoil coordinate
Y	Vertical coordinate

α	Angle of attack
β	$\beta = (1 - M_\infty^2)^{1/2}$
γ	Specific heat ratio; $\gamma = 1.4$
θ	Flow angle in vertical plane relative to control surface
ϕ	Velocity potential normalized by free-stream velocity

SUBSCRIPTS

E	Region exterior to the control surface
T	Measured value in wind tunnel